Lehigh University
Lehigh Preserve

Theses and Dissertations

1993

Simulation of charge pumping in scaled MOSFET devices

William E. Wagner
Lehigh University

Follow this and additional works at: http://preserve.lehigh.edu/etd

Recommended Citation
Wagner, William E., "Simulation of charge pumping in scaled MOSFET devices" (1993). *Theses and Dissertations.* Paper 186.

This Thesis is brought to you for free and open access by Lehigh Preserve. It has been accepted for inclusion in Theses and Dissertations by an authorized administrator of Lehigh Preserve. For more information, please contact preserve@lehigh.edu.

AUTHOR:

Wagner, William E., III

TITLE:

Simulation of Charge Pumping in Scaled MOSFET Devices

DATE: May 30, 1993

SIMULATION OF CHARGE PUMPING IN SCALED MOSFET DEVICES

by
William E. Wagner, III

A Thesis
Presented to the Graduate Committee
of Lehigh University
in Candidacy for the Degree of
Master of Science
in
Electrical Engineering

Lehigh University
May 21, 1993

This thesis is accepted and approved in partial fulfillment of the requirements for the Master of Science.

May 20, 1993
(date)

Dr. Marvin H. White
Thesis Advisor

Dr. Alastair D. McAulay
Chairman of Department

Acknowlegements

I would like to thank my advisor Dr. Marvin White for his support and guidance during the work on this thesis. He really sparked my interest in the field of device physics. He also provided a great environment to carry out research. The Sherman Fairchild Foundation provided the funding both for the summer program I participated in after my undergraduate graduation and for my work as a graduate student.

Many Thanks are due Dr. Richard Siergiej who introduced me to charge pumping, and provided much helpful guidance during my first year as a graduate student. He spent many hours working with me and answering my countless questions. Dr. Walter Dahlke and Dr. Daniel Leenov critiqued my work and gave their useful insights into the problems I faced. Their interest in the students and their desire to share their years of experience has greatly benefited the group.

It was my pleasure to work closely with Ronald Paulsen. His instructions on the operation of the experimental setup was greatly appreciated. He also aided my understanding of charge pumping. The processing would not have been possible without the oversight of Margaret French, Floyd Miller and Ray Filozof. Their willingness to take the time to train me and the time spent keeping the lab functional allowed the fabrication of the devices studied in this work.

Paul Orphanos and Matt Martin spent many hours maintaining the Sun workstations that were used for the computer simulations. I would also like to thank the other members of Dr. White's group: Amit Banerjee, Chun-Yu Malcolm Chen, Dr. Shexin Gong, Dr. Yin Hu, Zhigang Ma, Harikaran Sathianathan and Dr. Sukyoon

Yoon. I was glad to have the opportunity to work with this group. I had many fruitful discussions with the different students. I also enjoyed working with Lou Ballanca, Neil Cohen and Chris Kulp, who did research during the summer as undergraduate students. Mrs. Linda Dreisbach deserves special thanks for keeping all the administrative work under control.

I would like to thank my family for all their support over the years. From birth they provided me with a desire to learn and the opportunity to reach for my dreams.

Contents

Acknowlegements iii

List of Figures viii

List of Tables x

List of Symbols xi

Abstract 1

1 Introduction 2
- 1.1 Historical Review 2
- 1.2 Scope of this Thesis 6

2 Theory of Charge Pumping 8
- 2.1 Introduction 8
- 2.2 Capture and Emission of a Single Trap Level 8
- 2.3 Hole and Electron Recombination Currents 11
- 2.4 Change in Trap Potential 13
- 2.5 Charge Pumping Current 14
- 2.6 Theory of Two Level Charge Pumping 14
- 2.7 Theory of Tri-level Charge Pumping 19
- 2.8 Quantum Mechanical Considerations 22

3 Program Development 27
- 3.1 Introduction 27
- 3.2 Algorithm for Calculating Currents 28
- 3.3 Program Variations 32
- 3.4 Viewing the Output 33

4 **Waveforms** 35
4.1 Introduction 35
4.2 Two Level 36
4.3 Tri-Level 48
4.4 Quantum 48

5 **Computer Simulation** 53
5.1 Introduction 53
5.2 Two-Level Results 53
5.3 Tri-level 56
5.4 Quantization 57
5.5 Comparison to Fabricated Devices 59
5.6 Conclusions 61

6 **Conclusions** 63
6.1 Accomplishments 63
6.2 Suggestions for Future Work 63

References 66

A **Properties of Si** 71
A.1 Introduction 71
A.2 Band Gap 71
A.3 Carrier Concentration 72
A.4 Surface Potential vs. Gate Voltage 75

B **Fabrication Sequence** 80
B.1 The NMOS Processing Sequence 80

C **Experimental Setup** 83
C.1 Introduction 83
C.2 Charge Pumping 83

C.3 Determination of Flatband Voltage 85

D Derivation of Equations **86**

D.1 Capture and Emission Rates 86

D.2 Electron and Hole Currents 87

E Time of Simulations **90**

F Source Code **92**

F.1 `pump.h` 92

F.2 `pump.c` 94

Vitae **101**

List of Figures

1.1 Location of interface and bulk traps 3

1.2 Location of interface traps as a function of energy 4

2.1 The four processes that take place with Interface Traps 9

2.2 Probability of an electron becoming trapped is proportional to the capture cross section times the thermal velocity. 10

2.3 The charge pumping currents. I_1 and I_2 are the electron capture and emission components, respectively and I_3 and I_4 are the hole capture and emission components, respectively. 12

2.4 N-channel transistor under different biases 16

2.5 Waveforms used in two level charge pumping 18

2.6 Waveform used in tri-level charge pumping with step voltage on trailing edge. 20

2.7 Electrons from interface traps emit to E_0 instead of E_{CS}. 23

2.8 ΔE_O for different biases and doping levels at $300K$ and $77K$ 24

2.9 Ratio of 2D capture cross sections to 3D capture cross sections for different bias conditions and doping levels at $300K$ 25

3.1 Flow chart of main program used to simulate charge pumping 29

4.1 Waveform of square V_G used in two-level simulations 37

4.2 Waveform of ψ_s and ψ_t resulting from application of the waveform shown in figure 4.1 38

4.3 Waveform of hole and electron currents for the waveform of figure 4.1 . 39

4.4 ψ_s and ψ_t at 77 K for the square wave of figure 4.1 40

4.5 Currents at 77 K for the gate voltage of figure 4.1 41

4.6 Closeup of the rising edge of the waveform shown in figure 4.3 42

4.7 Surface and trap potentials for the currents shown in figure 4.6 . . . 43

4.8 Closeup of the falling edge currents of the waveform shown in figure 4.3 44
4.9 Surface and trap potentials for the currents shown in figure 4.8 . . . 45
4.10 ψ_s and ψ_t for an applied waveform of $\Delta V = 2.0V$ and $\Delta V = 3.0V$ . . 46
4.11 Currents corresponding to the potentials shown in figure 4.10 47
4.12 ψ_s and ψ_t not at equilibrium with a tri-level waveform applied to this device. 49
4.13 Currents not at equilibrium for the applied tri-level waveform, these currents correspond to the potentials shown in figure 4.12 50
4.14 ψ_s and ψ_t at equilibrium for the applied tri-level waveform. 51
4.15 Currents at equilibrium 51
4.16 Trap potential for the various combinations of two different capture cross sections and two different bulk biases 52

5.1 Q_{CP} as a function of frequency for sawtooth pulse ($\alpha = .5$). 54
5.2 Q_{CP} as a function of frequency for a square pulse 55
5.3 Q_{CP} for various base levels 55
5.4 Graph of Q_{CP} vs. step size for different step voltages 56
5.5 Graph of emission times 57
5.6 Graph of D_{it} as a function of trap level 58
5.7 Charge per cycle for differing values of bulk biasing 59
5.8 Simulation results compared to experimental data 60

A.1 Band Gap as a function of temperature for different doping levels . . 73
A.2 n_i as a function of temperature 74
A.3 Energy Bands of a n-channel semiconductor 76
A.4 Surface potential as a function of gate voltage at 300 K ($V_{SB} = 0$) . . 77
A.5 Surface potential as a function of gate voltage at different temperatures 79

C.1 Experimental setup 84
C.2 The MOS transistor from the TP-300 mask set used in the experiments 85

List of Tables

1.1 Comparison of interface trap measurement techniques.[1] 5

3.1 List of subroutines used in program 28
3.2 User supplied constants to simulation program (located in file pump.h) 30
3.3 Program calculated constants 30
3.4 Major subroutines 33
3.5 Output files 34

4.1 Constants used in simulations 35

5.1 Threshold and flatband Voltages found by varying the base level compared to theory 61
5.2 Summary of experiments for D_{it} and capture cross sections. 61
5.3 Summary of simulation of quantization effects 62
5.4 Comparison of experimental data to simulations with square wave pulses 62

A.1 Regions of operations of a n-channel semiconductor 76

E.1 Comparison of User times for simple two-level simulation on various machines 90
E.2 Comparison of User times for different simulations on *ratool*. 91

List of Symbols

c_n	rate of electron capture
c_p	rate of hole capture
e_n	rate of electron emission
e_p	rate of hole emission
f	frequency (s^{-1})
j_n	electron current density (A/cm^2)
j_p	hole current density (A/cm^2)
k	Boltzmann's constant ($1.38 * 10^{-23} J/K$)
h	Plank's constant ($6.63 * 10^{-34} Js$)
$\hbar$	Reduced Plank's constant ($h/2\pi$)
m_n^*	effective electron mass
m_p^*	effective hole mass
n_1	concentration of electrons in the trap
n_i	intrinsic density of electrons (cm^{-3})
n_o	electron density in the substrate (cm^{-3})
n_s	electron concentration at the surface
p_1	concentration of holes in the trap
p_o	hole density in the substrate (cm^{-3})
p_s	hole concentration at the surface
q	electron charge ($1.602 * 10^{-19} C$)
t	time
v_{th}	thermal velocity (cm/sec)
x_o	oxide thickness (cm)
C_{it}	interface trap capacitance(F/cm^2)
C_{ox}	oxide capacitance (F/cm^2)

D_{it}	density of interface traps $(cm^{-2}ev^{-1})$
I_{CP}	charge pumping current (A)
E_c	conduction band energy level
E_g	energy gap (eV)
E_{go}	energy gap assuming no band gap narrowing (eV)
E_v	valance band energy level
N_A	total number of acceptors (cm^{-2})
N_A^-	inonized acceptors (cm^{-2})
N_c	effective density of states at edge of conduction band (cm^{-3})
T	temperature (K)
Q_{CP}	charge pumping charge (C)
Q_s	semiconductor charge (C)
V_{FB}	flatband voltage (V)
V_g	applied gate voltage (V)
V_t	thermal voltage (kT/qV)
V_T	threshold voltage for strong inversion (V)
V_{Tweak}	threshold voltage for weak inversion (V)
ϵ_o	permittivity of free space $(8.85 * 10^{-19} F/cm)$
ψ_f	Potential far into the bulk (eV)
ψ_s	surface potential (eV)
ψ_t	interface trap potential associated with trap quasi-Fermi level (eV)
σ_n	capture cross section of electron (cm^2)
σ_p	capture cross section of holes (cm^2)
τ_e	emission time for electrons (s)
τ_f	fall time (s)
τ_h	emission time for holes (s)
τ_r	rise time (s)
ΔE_g	band gap narrowing (eV)

Abstract

Bi-level and tri-level charge pumping are widely used in the study of devices. These techniques allow the measurement of capture cross section and the density of states. This thesis describes how the computer simulations have been used to further the understanding of charge pumping. The program includes the effects of quantization of the conduction band. The simulations allow the actual waveforms to be examined. Experimental work does not allow the individual hole and electron currents to be viewed.

The simulations were carried out on a Sun SparcStation using standard C. It has also been tested on IBM RS600 workstations. The software is designed to be easily modified to incorporate other effects.

To confirm proper operation the results were compared to theories, which are also developed in this thesis. The simulations were then compared to devices that were fabricated in the lab. The devices were fabricated using the standard $2\mu m$ processing sequence.

Chapter 1

Introduction

1.1 Historical Review

As devices become smaller, variations in the device's parameters can change the performance of the device. Interface traps are among the effects of interest. Interface traps are created at the boundary between the Si and SiO_2 layers (please see figure 1.1). These traps exist over the entire energy range of the forbidden zone of the energy gap. By contrast, a bulk trap has one distinct energy level associated with it (see figure 1.2). A third type of traps are oxide traps. The effects of these traps are not included in this thesis.

Charge Pumping was first reported by Brugler and Jespers[2]. They investigated the two sources of the charge pumping current: the geometric component and the surface-state component. The surface-state component is the important effect in characterizing the interface traps. The geometric component results from the mobile charge recombining under the gate instead of traveling back to the source and drain[3]. It depends on the shape of the device under study. Brugler and Jespers [2] showed that when $W/L \gg 1$, few proportionally carriers will recombine before reaching the source or drain. In practice, the geometric component is minimized to improve the accuracy of the interface trap measurements. The geometric component is not included in the analysis presented in this thesis or in the simulation program. Groeseneken, Maes, Beltran and De Keersmaecker improved on the previous work

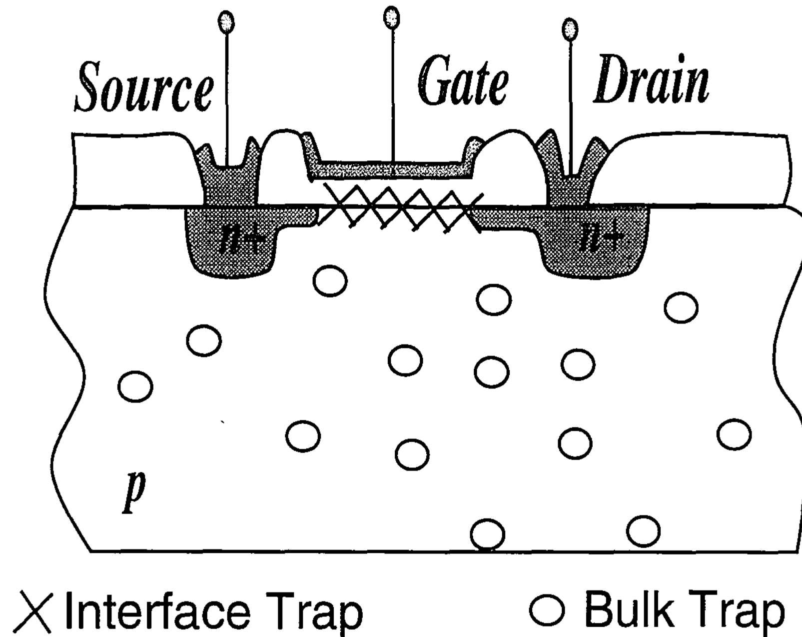

Figure 1.1: Location of interface and bulk traps

and developed a method to allow to the average interface state density, mean value of capture cross sections, and the distribution of interface states to be found[3]. The usefulness of charge pumping method was extended when Tseng introduced tri-level charge pumping [4]. Tri-level charge pumping allows more information to be gathered.

As table 1.1 shows, tri-level charge pumping is among the techniques that have the best D_{it}, density of interface traps, resolution. It also allows the capture cross sections (σ_n and σ_p) to be found for the same device. MOSFETs are harder to fabricate than capacitors due to the increased number of masks needed, so there are advantages to using the methods that only require capacitors. However, since the purpose of these investigation is to explain the performance of devices used in circuits, the transistor studies allow the results to be directly applied to the actual devices.

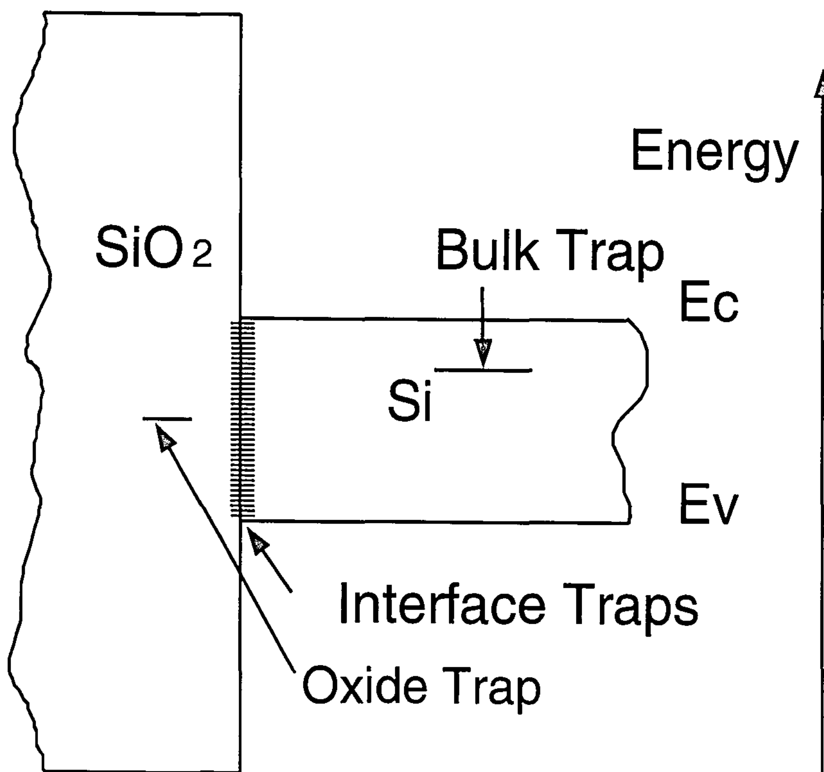

Figure 1.2: Location of interface traps as a function of energy

Measurement	Test Vehicle	Parameters	D_{it} Resolution
High freq. CV [5] (Termin's Method)	Capacitor	$D_{it}(E)$	10^{11}
Gray Brown CV [6]	Capacitor	$D_{it}(E)$	10^{11}
Quasi-Static CV [7, 8]	Capacitor	$D_{it}(E)$	10^{10}
Hi-Lo CV [8, 9]	Capacitor	$D_{it}(E)$	10^{10}
Conductance[10, 11]	Capacitor	$D_{it}(E)$,$\sigma_n(E)$ or $\sigma_p(E)$	10^9
Constant Capacitance-Deep Level Transient Spectroscopy [12, 13]	Capacitor	$D_{it}(E)$,$\sigma_n(E)$ or $\sigma_p(E)$	10^9
Electron Spin Resonance [14]	Bulk Si	$D_{it}(E)$	10^{12}
Gated Diode [15]	MOS structure	$\overline{D_{it}}$	10^{10}
Charge Pumping	MOSFET	$D_{it}(E)$,$\sqrt{\sigma_n \sigma_p}$	10^9
Tri-level CP	MOSFET	$D_{it}(E)$,$\sigma_n(E)$,$\sigma_p(E)$	10^9
g_m,I_{sub}[16]	MOSFET	$\overline{D_{it}}$	10^{11}, 10^{10}

Table 1.1: Comparison of interface trap measurement techniques.[1]

Charge pumping has been used to study the increase in interface traps after radiation[17], hot electron injection[18], and repeated cycling of MNOS memory devices[19]. It has also been used to investigate the reduction in trap density in MNOS devices after hydrogen annealing[20]. In practice, experiments measure the average current per cycle. It is not possible to see the actual current waveform as a function of time. However, computer simulations can show the waveform as a function of time. Viewing the waveforms allows a closer study of the charge pumping current and the individual contributions of the electrons and holes together with their emission and hole processes.

Processing of devices in the fabrication lab normally takes at least a month. However, changing the constants used in the program to simulate different devices takes a couple of minutes.

1.2 Scope of this Thesis

This work covers the development of the time domain analysis of the charge pumping current in MOS devices. The waveforms corresponding to the currents and potentials can be viewed. This gives more insight into the physical processes that are occurring in the device. This thesis covers the problems encountered in implementing the equations into a C program designed to run on Sun workstations, and how they were overcome.

Analytical techniques to study charge pumping are also developed. The two methods are compared to confirm that the simulations are actually producing reasonable results. Experimental results further attest to the accuracy of the results.

For the first time, the quantization effects that occur at high doping densities

have been included in computer simulations. The effects of emission to levels above the conduction band will increase in importance as devices become smaller. The effects of the quantization can be isolated and their effects can be investigated.

Chapter 2

Theory of Charge Pumping

2.1 Introduction

In order to simulate charge pumping the equations governing the device performance must be studied. Ghibaudo and Saks[21] derived the equations for the simulation for simple charge pumping experiments. The main advantage of this approach is that the currents flowing into the substrate and source and drain can be studied as a function of time. Analytical theories are also developed. These theories predict the expected results. These have been shown to be close to the actual values measured in experiments.

2.2 Capture and Emission of a Single Trap Level

Shockley-Read-Hall statistics [22, 23] statistics describe the capture and emission of holes and electrons from traps. The rate of capture of electrons into a trap at ψ_t, is the product of the capture cross section of the electron (σ_n), the thermal velocity (v_{th}), and the concentration of electrons at the surface (n_s) is shown by

$$c_n = \sigma_n v_{th} n_s \tag{2.1}$$

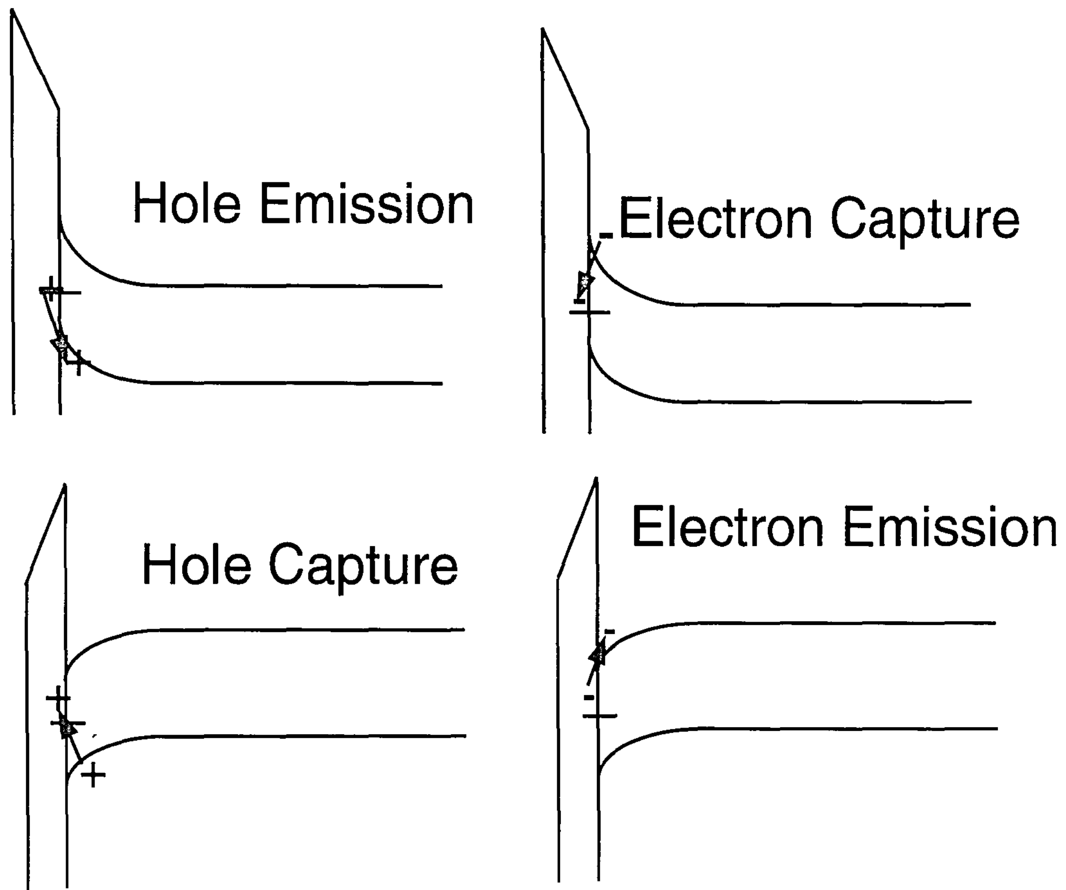

Figure 2.1: The four processes that take place with Interface Traps

where n_s is given by

$$n_s = n_o e^{q\psi_s/kT} \tag{2.2}$$

The rate of emission of electrons from the trap into the conduction band is

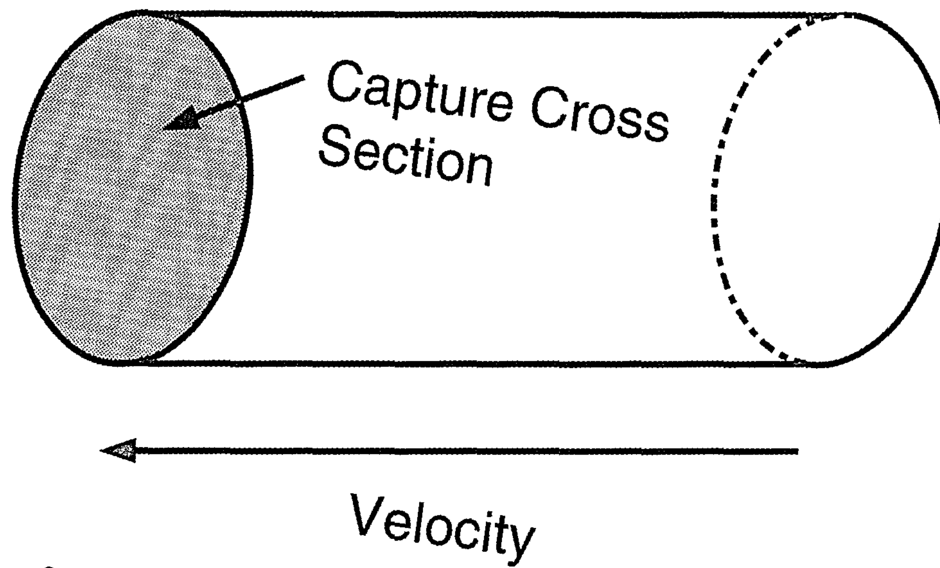

Figure 2.2: Probability of an electron becoming trapped is proportional to the capture cross section times the thermal velocity.

$$e_n = \sigma_n v_{th} n_1 \tag{2.3}$$

with n_1, the concentration of electrons in the trap, as follows

$$n_1 = n_o e^{q\psi_t/kT} \tag{2.4}$$

The equations relating to holes are similar and are shown below:

$$c_p = \sigma_p v_{th} p_s \tag{2.5}$$

$$p_s = p_o e^{q\psi_s/kT} \tag{2.6}$$

$$e_p = \sigma_p v_{th} p_1 \tag{2.7}$$

$$p_1 = p_o e^{-q\psi_t/kT} \tag{2.8}$$

where n_o and p_o are shown in section A.3. The thermal velocity also varies with temperature as follows [24]

$$v_{th} = \sqrt{\frac{8kT}{m_n^* \pi}} \tag{2.9}$$

In all these equations, v_{th} refers to the thermal velocity of the electron, with the variation of the thermal velocity with respect to holes and electrons included in the capture cross sections. Since, there are traps at every energy level between the conduction and valance level, equations 2.10 and 2.11 must be integrated over the entire energy band. It can be shown that only the traps within $\pi kT/2$ [1] of the trap level contribute to the current.

2.3 Hole and Electron Recombination Currents

The electron and hole recombination currents from a single trap level are equal to the net-rate of change of the trap charge multiplied by the number of states at that energy and the charge per particle.

$$j_n = C_{it}\frac{kT}{q}(e_n - c_n) \tag{2.10}$$

$$j_p = C_{it}\frac{kT}{q}(c_p - e_p) \tag{2.11}$$

with units of A/cm^2.

If there were no interface traps to store charge, the hole and electron currents would both sum to 0. Since charge can be stored in the trap, the currents will not sum to 0, however the currents over an entire cycle must have the same magnitude.

[1] Please see appendix D.2

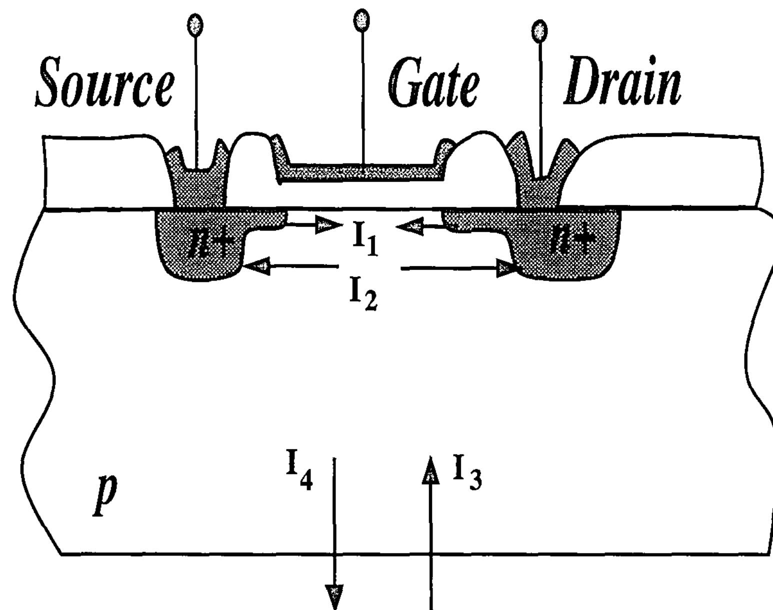

Figure 2.3: The charge pumping currents. I_1 and I_2 are the electron capture and emission components, respectively and I_3 and I_4 are the hole capture and emission components, respectively.

2.4 Change in Trap Potential

If the semiconductor is in equilibrium, the trap and surface potentials will be the same, $\psi_s = \psi_t$. Under these conditions, there will be no net electron or hole capture, so both the electron and hole currents will be zero. Most of the time the device will not be operating in equilibrium.

The differential interface trap charge is given by

$$\frac{\partial Q_{it}}{\partial \psi_t} = -C_{it} \tag{2.12}$$

The change in the interface trap charge is given by

$$\frac{dQ_{it}}{dt} = \jmath_p + \jmath_n \tag{2.13}$$

So, by applying equations 2.12, 2.11 and 2.10,

$$\frac{d\psi_t}{dt} = \frac{kT}{q}(c_n - e_n + e_p - c_p) \tag{2.14}$$

The Taylor expansion of ψ_t about t is

$$\psi_t(t + \Delta t) = \psi(t) + \frac{d\psi_t(t)}{dt}\Delta t + \frac{d^2\psi_t(t)}{dt^2}\frac{(\Delta t)^2}{2!} + \frac{d^3\psi_t(t)}{dt^3}\frac{(\Delta t)^3}{3!} + \cdots \tag{2.15}$$

If Δt is small,

$$\frac{d\psi_t(t)}{dt}\Delta t \gg \frac{d^2\psi_t(t)}{dt^2}\frac{(\Delta t)^2}{2!} + \frac{d^3\psi_t(t)}{dt^3}\frac{(\Delta t)^3}{3!} + \cdots \tag{2.16}$$

so expansion can stopped after the first two terms. Using equations 2.14 and 2.15, the value for ψ_t at some future time can be written as.

$$\psi_t(t + \Delta t) = \psi(t) + (\Delta t)\frac{d\psi_t}{dt} \tag{2.17}$$

2.5 Charge Pumping Current

The total current is the value of interest. It can be found either from the hole or electron current.

$$I_{cp} = \frac{1}{T_p}\int_0^{T_p} j_p(t)\,dt \tag{2.18}$$

$$= -\frac{1}{T_p}\int_0^{T_p} j_n(t)\,dt \tag{2.19}$$

where T_p is the time of each cycle.

2.6 Theory of Two Level Charge Pumping

In conventional two-level charge pumping, a repetitive pulse is applied to the gate of the MOS transistor (please see figure 2.5). If we consider a n-channel transistor, a voltage higher than V_T biases the transistor into inversion. The positive gate voltage pulls electrons toward the gate where they fill the interface traps between the Si and SiO_2 If the lower voltage is below V_{FB}, the device will be biased into accumulation. Since the gate is composed of SiO_2, an insulator, the current flowing through the gate is much smaller than the currents flowing through the source, drain and the substrate. The source and drain supply the electron current, and the hole current is supplied by the substrate (please see figure 2.3). As stated previously, we are assuming that the geometric component is negligible.

At the start of the cycle when $V_L < V_{FB}$ is applied the device will be in accumulation, and traps will be empty of electrons. As the voltage increases from $V_L < V_{FB}$

to $V_H > V_T$, holes will start to emit from the traps to the valence band. As long, as the voltage is low enough, the device will be operating in steady-state. At a gate voltage close to flatband, a transition to non-steady state will occur. As the pulse continues to rise, the device will be operating in the depletion region. Since, there are few free carriers, the rate of emission of holes will set the trapping time constant. Close to weak inversion, the electrons will be captured into traps that are still occupied by holes. This results in Recombination of an electron-hole pair. When the device is in strong inversion all the traps will be filled and the device will once again be in equilibrium. When the voltage pulse descends, electrons will start to emit back to the conduction band. When the device is the depletion region, the electron emission becomes less than the capture of holes, once again resulting in Recombination. Finally, the device will reach equilibrium in accumulation and the process will start over. The current can be measured through either the electrons moving through the source and drain or the holes moving through the substrate of the device.

The current is averaged over the cycle and from the current, various parameters can be determined. Groeseneken, et al.[25] have developed equations for the behavior of devices under simple two-level charge pumping experiments. Assuming the base voltage level is V_L, the amplitude is ΔV_G, the rise and fall transient times (assumed to be independent of the frequency, f) are t_f and t_r, the maximum current per unit area is for n-channel

$$I_{CP} = 2q\overline{D_{it}}kTf\left[\ln(v_{th}n_i\sqrt{\sigma_n\sigma_p}) + \ln(\frac{\mid V_{FB} - V_T \mid}{\mid \Delta V_G \mid}\sqrt{t_f t_r})\right] \quad (2.20)$$

The charge per cycle Q_{CP} which can be written as

$$Q_{CP} = \frac{I_{CP}}{f} = 2q\overline{D_{it}}kT\left[\ln(v_{th}n_i\sqrt{\sigma_n\sigma_p}) + \ln(\frac{\mid V_{FB} - V_T \mid}{\mid \Delta V_G \mid}\sqrt{t_f t_r})\right] \quad (2.21)$$

will remain constant as a function of frequency.[2] These equations assume that

[2]Recent work suggests that near-interface oxide traps cause Q_{CP} to increase at low frequencies[26]. These traps are located in the bulk of the SiO_2, but close to the surface. Paulsen showed that interface to bulk dielectric trap tunneling explains these results.[27]

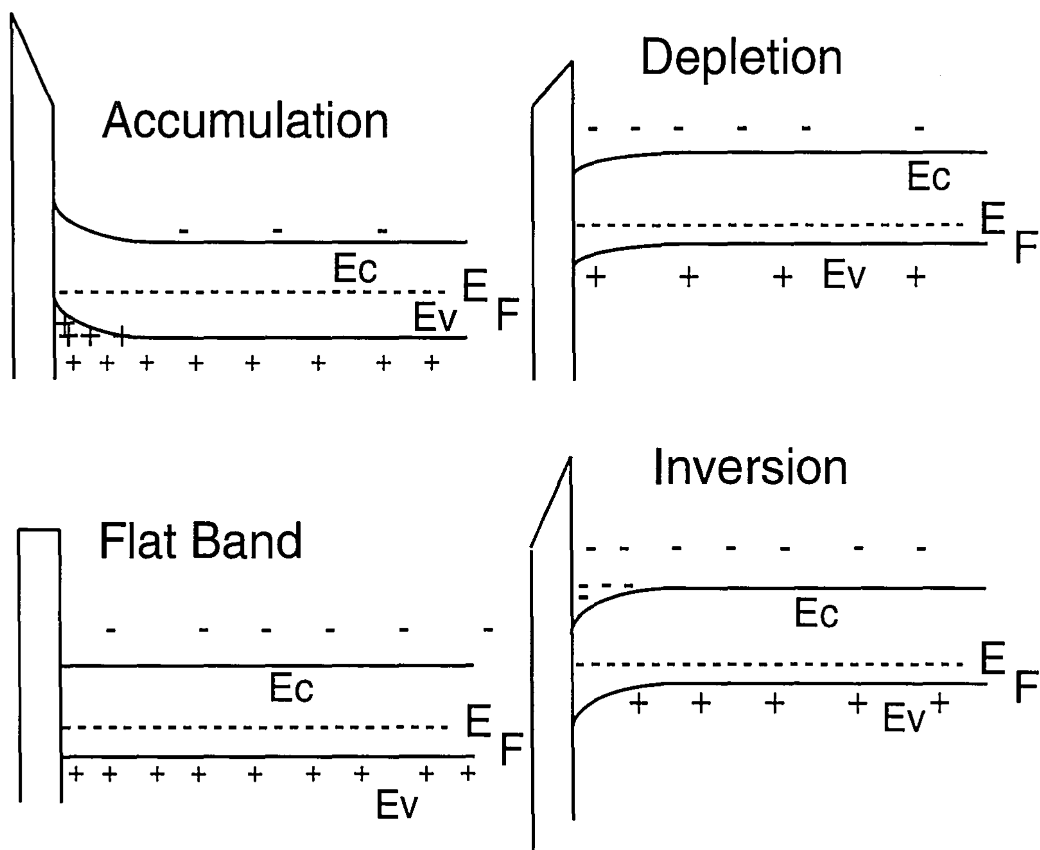

Figure 2.4: N-channel transistor under different biases

$V_L < V_{FB}$ and $V_H = V_L + \Delta V_G > V_T$. If the entire region from V_{FB} to V_T is not scanned, the current will be less than the value given in 2.20.

In the experiments performed in our lab, ΔV_G is is set so that

$$\Delta V_G > V_T - V_{FB} \tag{2.22}$$

and the base voltage is swept from a value below $V_{FB} - \Delta V_G$ to a value above V_T. The maximum value of I_{CP} is used to determine $\overline{D_{it}}$ by applying equation 2.20. The values of V_L that correspond to the locations where the current is half of its maximum value are $V_{TH} - \Delta V_G$ and V_{FB}. The values obtained for V_{TH} and V_{FB} by this method are not very accurate and are generally used only as a check that they are reasonable.

Another useful technique, also from Groeseneken[25] is to use a sawtooth wave as the applied signal. The high voltage is set so $V_H > V_T$ and the low voltage is set so $V_L < V_{FB}$. The waveform consists of two sections. During the first α fraction of the pulse width the voltage is linearly increasing from V_L to V_H and during the remaining $1 - \alpha$ is linearly decreases. The equation for Q_{CP} can be derived from 2.20 as follows:

$$t_r \rightarrow \frac{\alpha}{f} \tag{2.23}$$

$$t_f \rightarrow \frac{1-\alpha}{f} \tag{2.24}$$

$$\Rightarrow Q_{CP} = 2q\overline{D_{it}}kT\left[\ln(v_{th}n_i\sqrt{\sigma_n\sigma_p}) + \ln(\frac{\mid V_{FB} - V_T \mid}{\mid \Delta V_G \mid}\frac{1}{f}\sqrt{\alpha(1-\alpha)})\right] \tag{2.25}$$

From the sawtooth pattern, both $\sqrt{\sigma_n\sigma_p}$ and $\overline{D_{IT}}$ can be found. If $Q_{CP} = 0$ in (2.25),

$$\sqrt{\sigma_p\sigma_n} = \frac{1}{v_{th}n_i}\frac{\mid \Delta V_G \mid}{\mid V_{FB} - V_T \mid}\frac{f}{\sqrt{\alpha(1-\alpha)}} \tag{2.26}$$

Also,

$$\frac{dQ_{CP}}{d\log f} = \frac{2qkT\overline{D_{IT}}}{\log e} \tag{2.27}$$

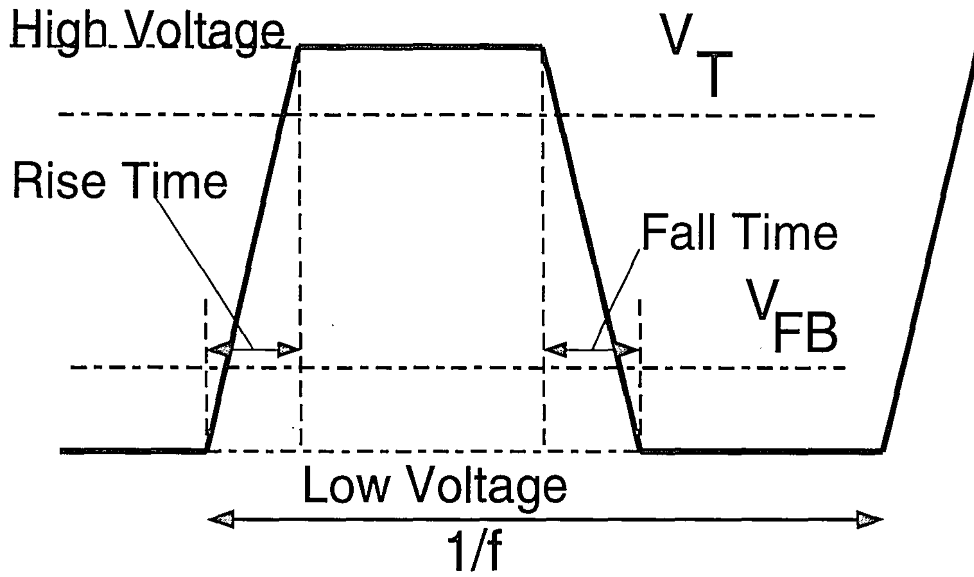

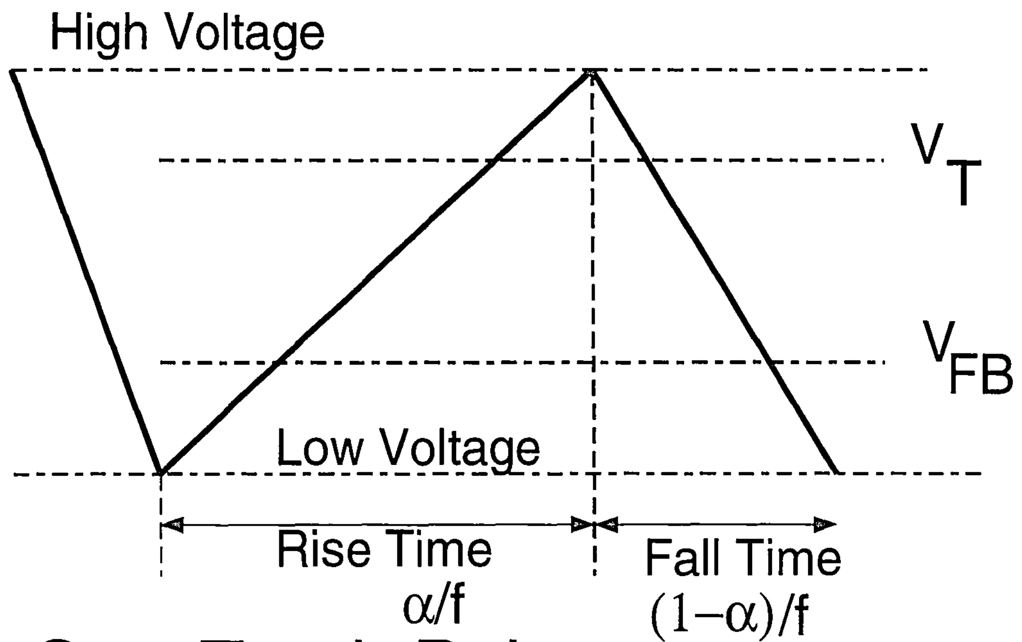

Figure 2.5: Waveforms used in two level charge pumping

which leads to a value of $\overline{D_{IT}}$.

The equations for Q_{CP} developed in this section, were done assuming the transition from steady state to non-steady state occurs when $V_G = V_{FB}$ and that the transition from non-steady state to steady-state is when $V_G = V_{TH}$. Groeseneken justified these approximations in his paper [25].

The derivation of the equations in this section was done independent of the time-domain analysis method of determining the charge pumping current, thus equations 2.20 and 2.25 can be used to verify the operation of the simulator.

2.7 Theory of Tri-level Charge Pumping

Tri-level charge pumping expands two-level charge pumping to allow more information to be gathered. In addition to the voltage above the threshold voltage and the voltage below flat-band (both held long enough to reach equilibrium), a third voltage V_{step} is applied so that

$$V_{FB} < V_{step} < V_T \tag{2.28}$$

This step voltage is either applied either before or after the device is brought into accumulation. If the mid-voltage is applied following the high voltage, the electrons will start to emit back to the conduction band. If the time is long enough all the traps above the trap level will be empty of electrons, while all the traps below this level will be filled. The charge that remains gets recombined when the surface is inverted. The more electrons that were re-emitted to the conduction band the lower the recombination current will be. The time the device is held at this level, t_{step}, is varied to allow study of the states at the energy level being probed. The pulse is applied either to the leading edge or the trailing edge of the high voltage pulse.

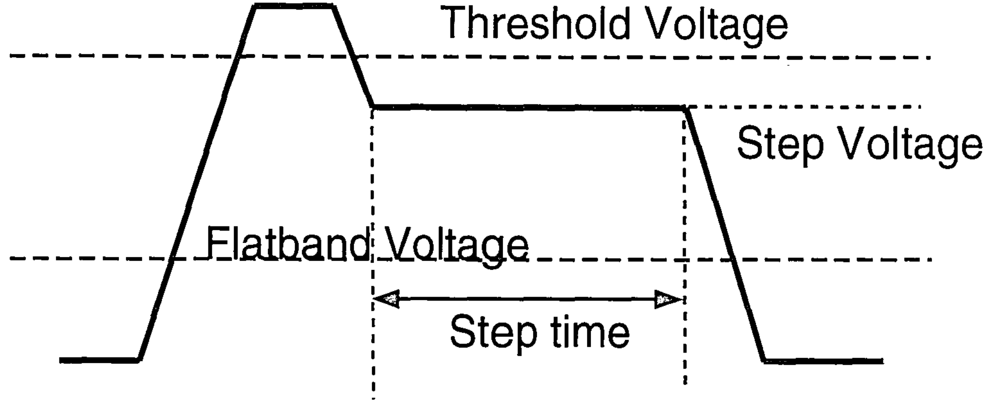

Figure 2.6: Waveform used in tri-level charge pumping with step voltage on trailing edge.

When the the pulse is on the trailing edge the upper part of the energy gap is investigated.

For the case of electron emission the total charge recombining with holes from the conduction band is[1]

$$Q_t = q\overline{D_{it}}E_m(t) \tag{2.29}$$

where $E_m(t)$ is the energy of the uppermost-filled trap level referenced to the valance band. It is given by[28]

$$E_m(t) = E_t - kT\ln[1 - (1 - e^{(E_t - E_{CS})/kT})]e^{-(t_{step}+t_f)/\tau_e} \tag{2.30}$$

Where $\tau_e = e_n^{-1}$ (see equation 2.3) is the time constant of the emission of electrons.

The total current is just the charge per cycle multiplied by the frequency.

$$I_{CP} = fQ_t \tag{2.31}$$

$$= fq\overline{D_{it}}E_m(t) \tag{2.32}$$

As the step time approaches 0, the current approaches the value given by the two-level experiment equation 2.20 where $E_t = E_i$. This equation is independent of the

value of the step voltage. As the step time increases the current will saturate at a final value of

$$I_{CP}(t_{STEP} \rightarrow \infty) = fq\overline{D_{it}}E_t \quad (2.33)$$

This enables one to find the trap energy level, E_t, when $\overline{D_{it}}$ is known.

A plot of I_{CP} vs. $\log(t)$ has a breakpoint at τ_e. Once τ_e and E_t are known, the capture cross section for a particular energy level can be found from

$$\sigma_n = \frac{e^{(E_{CS}-E_t)/kT}}{\tau_e v_{th} N_C} \quad (2.34)$$

If the pulse is instead placed on the leading edge, then a similar analysis can be used to find τ_h and σ_p. By solving the rate equations, analytical expressions for τ_e and τ_h are found to be[1]

$$\tau_e = \frac{1}{\sigma_n v_{th} N_c} e^{(E_C-E_t)/kT} \quad (2.35)$$

$$\tau_h = \frac{1}{\sigma_p n_{th} N_v} e^{(E_t-E_V)/kT} \quad (2.36)$$

When $\tau_e = \tau_h$, $E_t = E_{TP}$, where E_{TP} is the pinning level (The energy level where maximum electron-hole pair generation occurs). The equation for E_{TP} can be developed as follows:

$$\tau_e = \tau_h \quad (2.37)$$

$$e^{(E_C-2E_{TP}+E_V)/kT} = \frac{\sigma_n N_c}{\sigma_p N_v} \quad (2.38)$$

since everything is referenced to E_v and $E_c - E_v = E_G$,

$$e^{(E_g-2E_{TP})/kT} = \frac{\sigma_n N_c}{\sigma_p N_v} \quad (2.39)$$

$$\frac{E_g + 2E_{TP}}{kT} = \ln\frac{\sigma_n}{\sigma_p} + \ln\frac{N_c}{N_v} \quad (2.40)$$

$$E_{TP} = -\frac{kT}{2}\ln\frac{\sigma_n}{\sigma_p} + \frac{E_G}{2} - \frac{kT}{2}\ln\frac{N_c}{N_v} \quad (2.41)$$

Since $\frac{E_g}{2} + \frac{kT}{2}\ln N_c/N_v \triangleq E_i$,

$$E_{TP} - E_i = -\frac{kT}{2}\ln\frac{\sigma_n}{\sigma_p} \tag{2.42}$$

States close to the pinning level are hard to probe. Very slow waveforms must be used because the time constants will be large. Tseng [4] developed an expression for calculating $D_{it}(E)$ by looking at the current at two different step levels as shown below:

$$D_{it}(\psi_{step}) = \frac{1}{qf}\frac{\mid \Delta I_{CP} \mid}{\mid \psi_{step1} - \psi_{step2} \mid} \tag{2.43}$$

2.8 Quantum Mechanical Considerations

Siergiej has extended the knowledge of interface traps by considering the quantization of energy levels in the conduction band[1]. Previous work considered the interface traps to emit to the lower edge of the conduction band. However, Siergiej showed the electrons actually emit to the first quantization level (please see figure 2.7), E_0, where

$$E_0 = E_{CS} + \Delta E_0 \tag{2.44}$$

$$\Delta E_0 \approx (\frac{\hbar^2}{2m_l})^{1/3}(\frac{9}{8}\pi q \mathcal{E}_s)^{2/3} \tag{2.45}$$

The surface electric field, $\mathcal{E}_s$ can be found from

$$\mathcal{E}_s = \frac{Q_B + Q_{inv}}{K_s \epsilon_o} \tag{2.46}$$

where

$$Q_{inv} \approx C_{ox}(V_{GS} - V_T) \tag{2.47}$$

$$Q_B \approx \sqrt{2K_S\epsilon_o q N_B(V_{SB} + 2\psi_F)} \tag{2.48}$$

if we assume $V_{DS} \approx 0$. In charge pumping experiments the source and drain are generally tied together, so this condition will be satisfied. The effect of the quan-

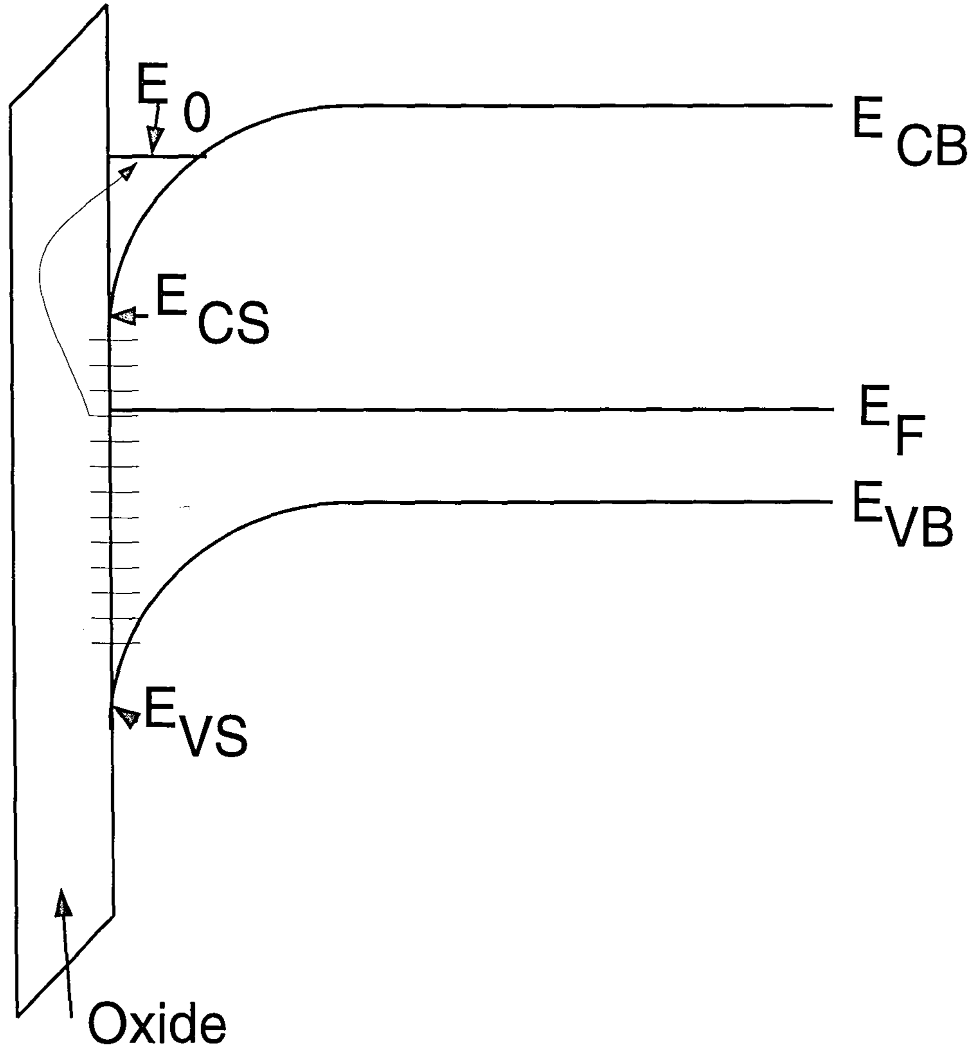

Figure 2.7: Electrons from interface traps emit to E_0 instead of E_{CS}.

tization changes the effective capture cross section for electrons[1].

$$\sigma_n(2D) = \frac{N_C(3D)}{N_C(2D)} \frac{e^{\Delta E_0/kT}}{\sqrt{\Delta E_0/kT}} \sigma_n(3D) \tag{2.49}$$

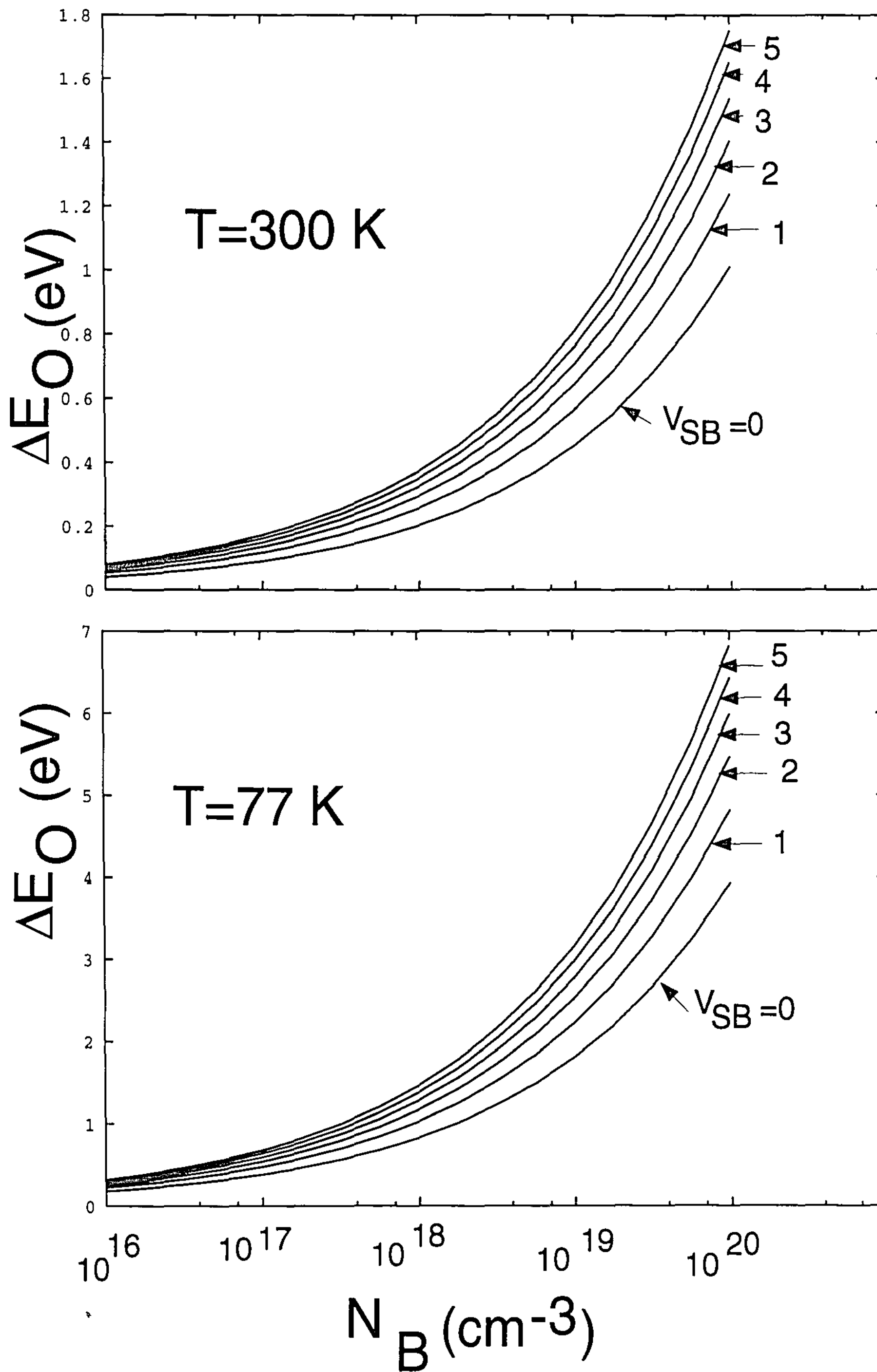

Figure 2.8: ΔE_O for different biases and doping levels at $300K$ and $77K$

$$\approx \quad 3.55 \frac{e^{\Delta E_0/kT}}{\sqrt{\Delta E_0/kT}} \sigma_n(3D) \qquad (2.50)$$

Different bulk biases produce different emission times, however as long as the same

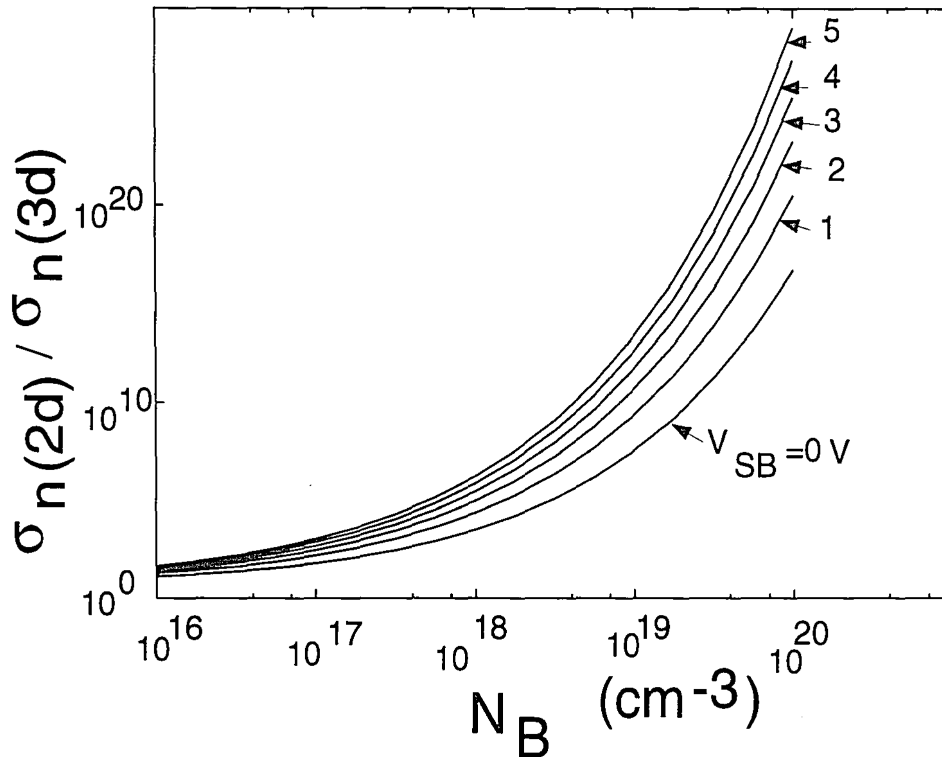

Figure 2.9: Ratio of 2D capture cross sections to 3D capture cross sections for different bias conditions and doping levels at $300K$

trap level is being probed the final current values should be the same. The ratio of emission times can be expressed as

$$\ln(\frac{\tau_{e1}}{\tau_{e2}}) = \frac{\alpha}{kT}[(2\psi_f + V_{SB1})^{1/3} - (2\psi_f + V_{SB2})^{1/3}] \qquad (2.51)$$

where

$$\alpha = (\frac{\hbar^2 q N_B}{K_S \epsilon_o m_l})^{1/3} (\frac{9\pi q}{8})^{2/3} \qquad (2.52)$$

The quantum effects associated with the holes and the valence bands have much faster time constants, so they are not considered in this work.

The ratio of capture cross sections was done with the assumption that the first quantization level was constant. The level is dependent on the electric field and will vary as the gate voltage changes. The simulation program treats the capture cross section as a constant. When the currents are viewed it will be shown that most of the emission takes place when the gate pulse is at a fixed value.

Chapter 3

Program Development for Computer Simulation of Charge Pumping Experiments

3.1 Introduction

The results of the previous section can be easily applied to a computer routine to simulate charge pumping, since the computer can carry out millions of operations each second. The program used in this thesis was written in standard C, and run on a Sun workstation. It was also run on IBM RISC System/6000 work stations. On both systems, speed was a major problem especially for the long tri-level simulations (see E for the times of the simulations). Since many calculations are involved and much memory is needed, these programs were not even attempted on slower machines such as personal computers.

Many of the numbers used in the program are small. In order to provide accurate results it was necessary to use double precision numbers. The use of double precision numbers slows down the calculations, but in this case they are needed.

3.2 Algorithm for Calculating Currents

Subroutine	Function
calc_constants	Calculates band gap, intrinsic doping density, Thermal velocity, and capture cross sections
calc_jp	Returns hole current at a given time
calc_jn	Return electron current at a given time
calc_dpsit	Returns change in trap potential
f	Returns $f(u_s)$
qs	Returns semiconductor charge (Q_s)
calc_vg	Returns gate voltage for a given surface potential
calc_vgtpsis	Calculates table of gate voltage and surface potential
calc_psis	Looks up surface potential for given gate voltage
return_vg	Returns gate voltage at the given time
fwopen	Opens the files and checks for errors
calc_i	Returns total charge per cycle for chosen waveform
main	The main program

Table 3.1: List of subroutines used in program

The first task the program performs is to calculate the various constants used in the program. E_g, n_i, n_o, p_o, etc. vary with the temperature and the doping level of the device, but they remain constant for the duration of the simulation.

The next task is to calculate a table of ψ_s vs. V_G using equation A.15. This speeds up the execution of the program, since it is impossible to determine ψ_s from V_G without using an iterative approach. The program calculates V_G for 1000 values (this value can be changed via the POINTS constant in the *pump.h* file) of ψ_s between ψ_{smin} and ψ_{smax}. The value of 1000 was picked to allow ψ_s to be found

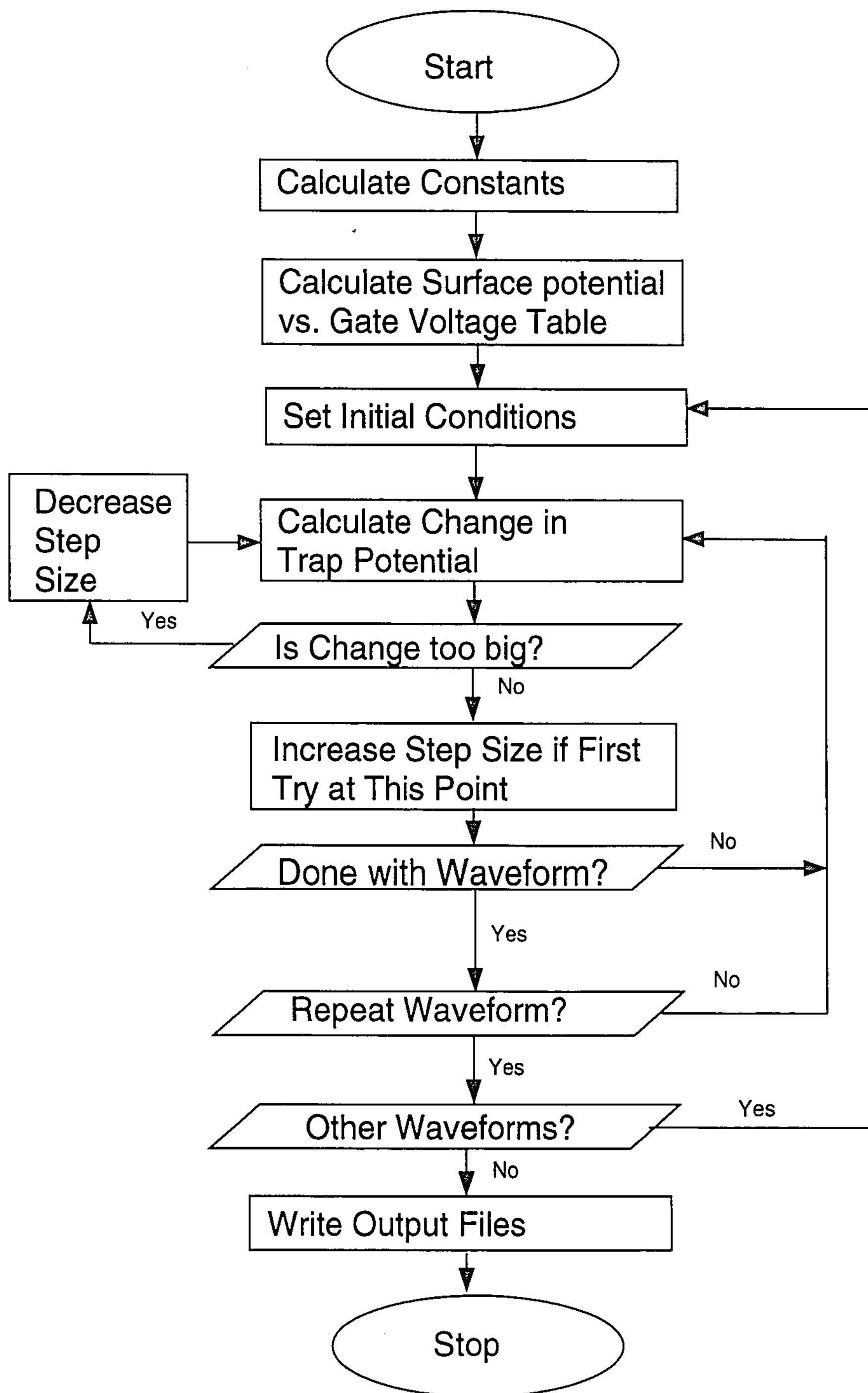

Figure 3.1: Flow chart of main program used to simulate charge pumping

Constants Name	Symbol	Meaning
NA	N_A	Acceptor Doping Density
NIT	N_{it}	Number of Interface traps per eV
SN	σ_n	3D Capture Cross Section of electrons
SP	σ_p	3D Capture Cross Section of holes
T	T	Temperature
VFB	V_{FB}	Flat Band Voltage
VSB	V_{sb}	Bulk Bias
XO	x_o	Oxide Thickness
COUNT		Number of times to run through waveform
POINTS		Number of Points in V_G vs. ψ_s table

Table 3.2: User supplied constants to simulation program (located in file pump.h)

Constant Name	Symbol	Equation
CIT	C_{it}	A.24
COX	C_{ox}	A.17
EG	E_G	A.1 & A.3
LD	L_D	A.21
NI	n_i	A.4
PO	p_o	A.9
NO	n_o	A.10
UF	u_f	A.23
VT	V_t	A.18
VTH	v_{th}	2.9
PSIMAX	ψ_{smax}	A.25
PSIMIN	ψ_{smin}	A.26

Table 3.3: Program calculated constants

accurately enough while not using too many points which would slow down the system.

Initially the device is assumed to be in accumulation and equilibrium so

$$\psi_t(0) = \psi_s(0) \tag{3.1}$$

where $\psi_s(0)$ is found from $V_G(0)$ and the ψ_s vs. V_G table calculated previously.

Once the initial value is known for ψ_t, equation 2.17 can be used to find the value of ψ_t for the next time value. Care must be taken to make sure the value used for Δt is not too large. However a too small value is not good either since it slows down the computer. After study it was decided that a variable time step would be best. Initially the program, chooses a step size equal to the time of initial transition from accumulation to inversion divided by 25[1]. This value was picked through trial and error as the largest time step that produced good results. The computer will adjust this step size if the current value is either too high or too low. It calculates a value for $\psi_t(t + \Delta t)$ and also a value for $\psi_t(t + \Delta t/2)$. From the $\psi_t(t + \Delta t/2)$ value it re-calculates the value for $\psi_t(t + \Delta t)$. If the two values of $\psi_t(t + \Delta t)$ differ by more than $(\psi_{smax} - \psi_{smin})/1000$ then the step size is reduced by a factor of ten and the program attempts the problem again. Again, the number 1000 was determined through trial and error, but this method seems to produce values of q_n and q_p that were closest to each other for the entire cycle. If the computer did not have to scale back the time step, the time step is multiplied by 5 before the next step is taken. The computer is limited to a maximum step size of 4 times the initial step size. Higher values caused the j_n and j_p values to differ from each other.

The computer integrates both the hole and electron currents over the time cycle. It uses Simpson's rule to approximate the integral. The differential charge is

[1] If the simulation is saving the waveforms the step size is reduced by 10. This produces smoother graphs for the currents and potentials but the large step size still produces results that are off by less than 1% for the overall charge. In the case of a sawtooth wave, the transition time of the rising edge is divided by 2500. .

expressed as follows

$$\Delta q_n = \frac{\Delta t}{6}\left[j_n(t) + 4j_n(t+\frac{\Delta t}{2}) + j_n(t+\Delta t)\right] \tag{3.2}$$

$$\Delta q_p = \frac{\Delta t}{6}\left[j_p(t) + 4j_p(t+\frac{\Delta t}{2}) + j_p(t+\Delta t)\right] \tag{3.3}$$

This method produced good results, and was more stable than the trapezoidal rule method.

Over a complete time cycle, I_{cp} should be the same no matter whether j_n or j_p was summed to calculate it (equations 2.19 and 2.18). This provides a convenient check to make sure the program is producing reasonable results.

To improve the accuracy of the simulation, the entire waveform is simulated multiple times. It was found that simulating the waveforms four times, produced results that were more stable than just a single time. This results since the step size has already been adjusted and the effects of the computer's lack of precision with small numbers cancelling itself out with more points. Once again, there are tradeoffs between increased accuracy and the computer time needed.

3.3 Program Variations

While the basic technique remains the same, different versions of the program are used to carry out the different simulations. The main routine calls one of the subroutines listed in table 3.4.

Subroutine	What it simulates
varybase	two-level waveform, vary base voltage
varyfreq	two-level waveforms vary frequency
tri	tri-level waveforms

Table 3.4: Major subroutines

3.4 Viewing the Output

The computer produces various output files, depending on what simulation was run. The computer places comments at the head of the data. The output files are designed to be used with Gnuplot[2] Gnuplot expects the data to be in x y format with comments lines marked with '#' at the start of the line. The program places comment lines at the start of each file listing the key parameters for the simulation. The data file could be used by other programs (like IslandChart, Lotus 123 and Borland Quattro) that accept standard ASCII format. Gnuplot can be used to create postscript files that can be printed or further enhanced by other programs. The graphs in this thesis were further enhanced by IslandDraw.

Gnuplot can also be used to plot out error bars. If a third number is added after the x y data, then the number is assumed to be the possible error in y. The program takes advantage of this when saving the current data. The y value is taken to be the average of the magnitude of the hole and electron components. The error is taken to be the difference in the magnitudes. This provides a check that the values are

[2]Gnuplot is a shareware program. It copyrighted by Colin Kelley and Thomas Williams, but they allow users to freely distribute the source code as long as the person copying the software agrees to a few basic conditions. As a result this package is available on many types of computer systems.

correct.

File Name	Contents
curr.dat	$Q_{CP}(V_L)$
currf.dat	$Q_{CP}(f)$
jn.dat	$j_n(t)$
jp.dat	$j_p(t)$
psis.dat	$\psi_s(t)$
psit.dat	$\psi_t(t)$
vg.dat	$V_g(t)$
vgt	ψ_s vs. V_g

Table 3.5: Output files

Chapter 4

Computer Generated Waveforms

4.1 Introduction

Simulations have been carried out to check the accuracy of the simulations. The results are all close to what was predicted. The current waveforms can not be directly compared to experimental data, but they can be compared to theoretical data. Unless otherwise specified, the user supplied constants (please see table 3.2 for the descriptions) used in the following simulations are given in table 4.1. The

Constant	Value
NA	10^{16}
NIT	10^{10}
SN	10^{-17}
SP	10^{-17}
T	300
VFB	0
XO	10^{-6}
VSB	0

Table 4.1: Constants used in simulations

graph of surface potential and gate voltage for these conditions is shown in figure

A.4. The quntization effects were only simulated in the quantization section, since these effects are handled by changing the capture cross sections of the devices.

4.2 Two Level

The gate voltage shown in figure 4.1 was simulated. The graph of the surface and trap potentials are shown in graph 4.2. The surface potential follows the gate voltage exactly, while the trap potential takes time to catch up.

The hole and electron currents are also shown. When $j_n > 0$ electrons are emitting and when $j_n < 0$ electrons are being captured. For holes $j_p > 0$ is hole capture and $j_p < 0$ is hole emission. When ψ_s and ψ_t are far enough apart the currents become saturated and stay at that value until ψ_t can catch up with ψ_s.

At lower temperatures with the same applied voltage, the surface potential changes a larger amount (figure 4.4). However, due to the decreased thermal velocity, fewer carriers, and fewer traps contributing to the current, it takes longer for the trap potential to catch up. In the example shown, the trap potential does not reach the surface potential and equilibrium is not reached. Figure 4.5 shows the hole and electron capture for this simulation. The electron current remains at its maximum value until the voltage on the gate changes. This is expected since the trap potential is changing linearly, and is not equal to the surface potential during the high gate pulse.

If we look at the rising edge waveform close up shown in figure 4.6 and the associated graph of the potentials in figure 4.7, we can see the distinct stages. First, the holes are emitted. While holes are still emitting, the traps start to capture electrons. When the trap potential, reaches the flatband voltage ($\psi_t = 0$) the

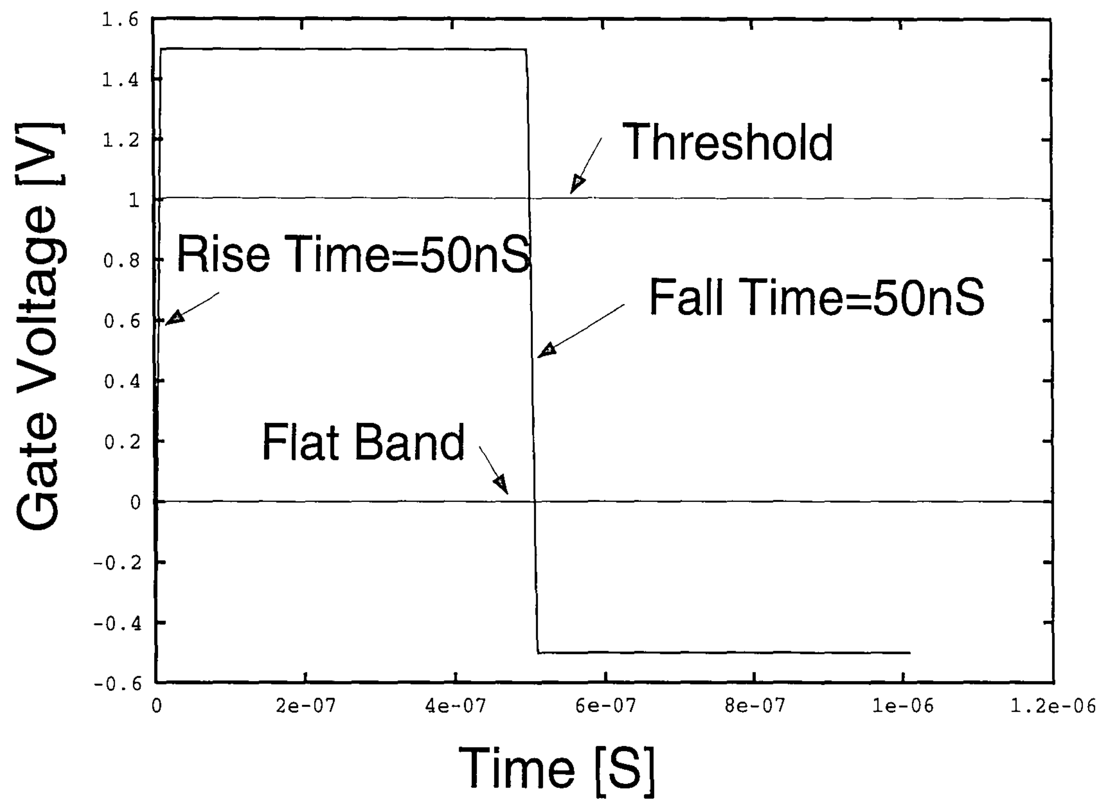

Figure 4.1: Waveform of square V_G used in two-level simulations

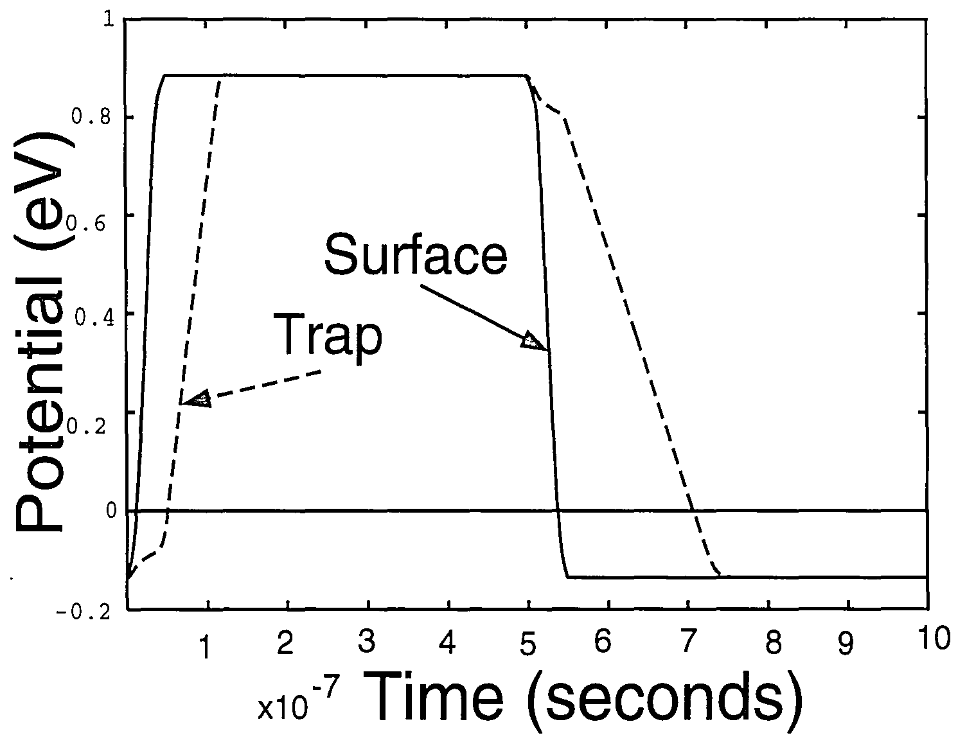

Figure 4.2: Waveform of ψ_s and ψ_t resulting from application of the waveform shown in figure 4.1.

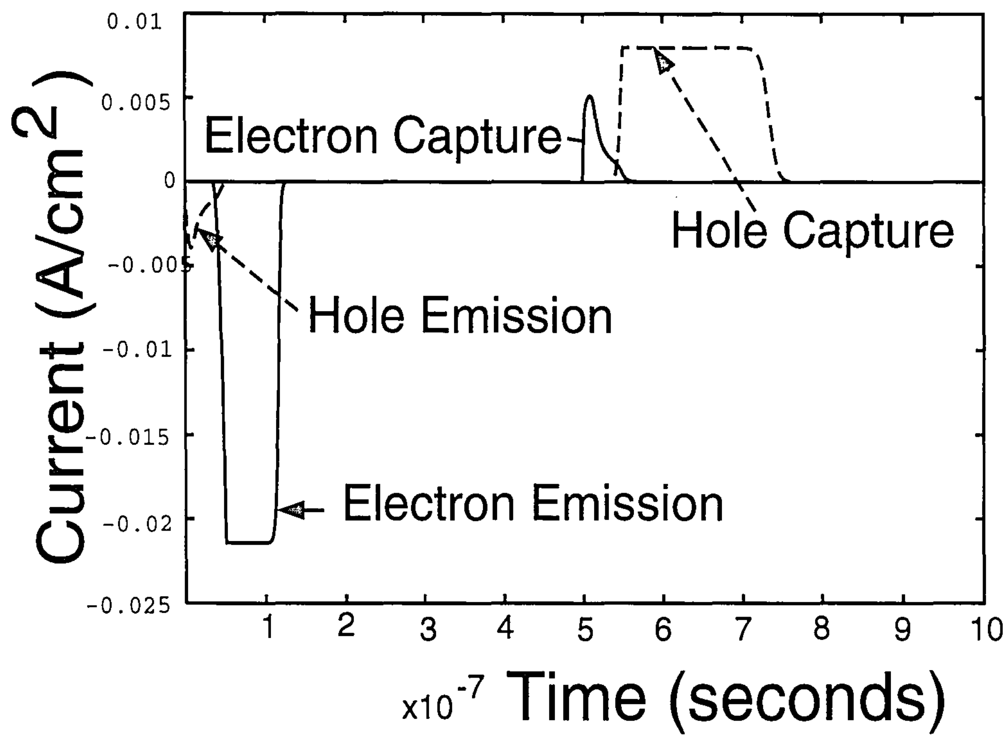

Figure 4.3: Waveform of hole and electron currents for the waveform of figure 4.1.

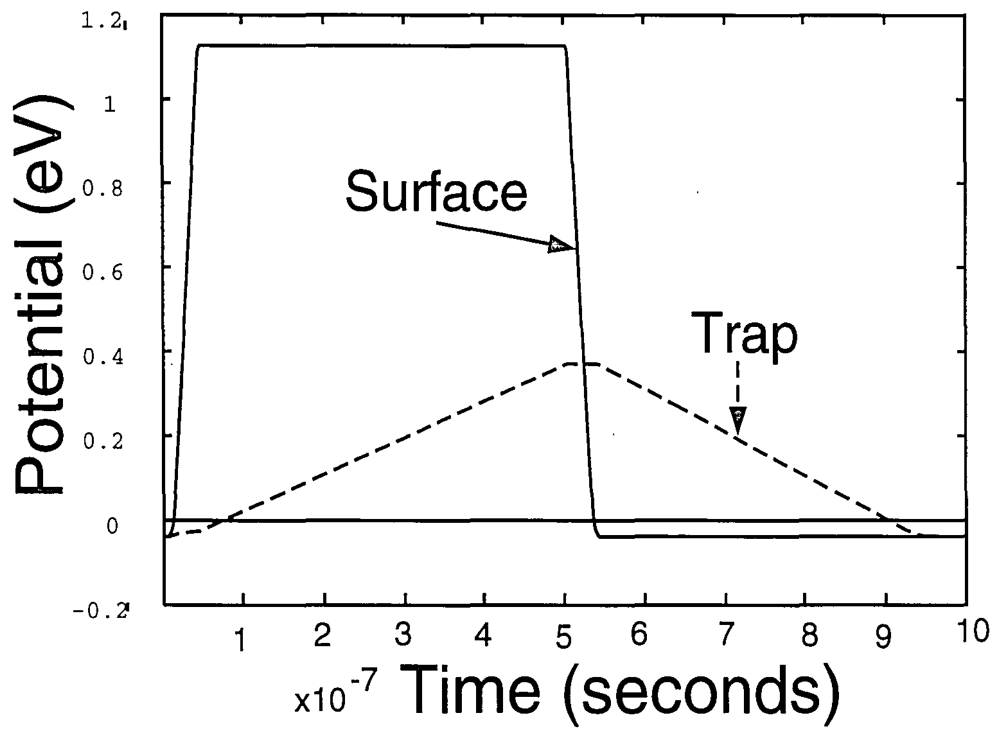

Figure 4.4: ψ_s and ψ_t at 77 K for the square wave of figure 4.1.

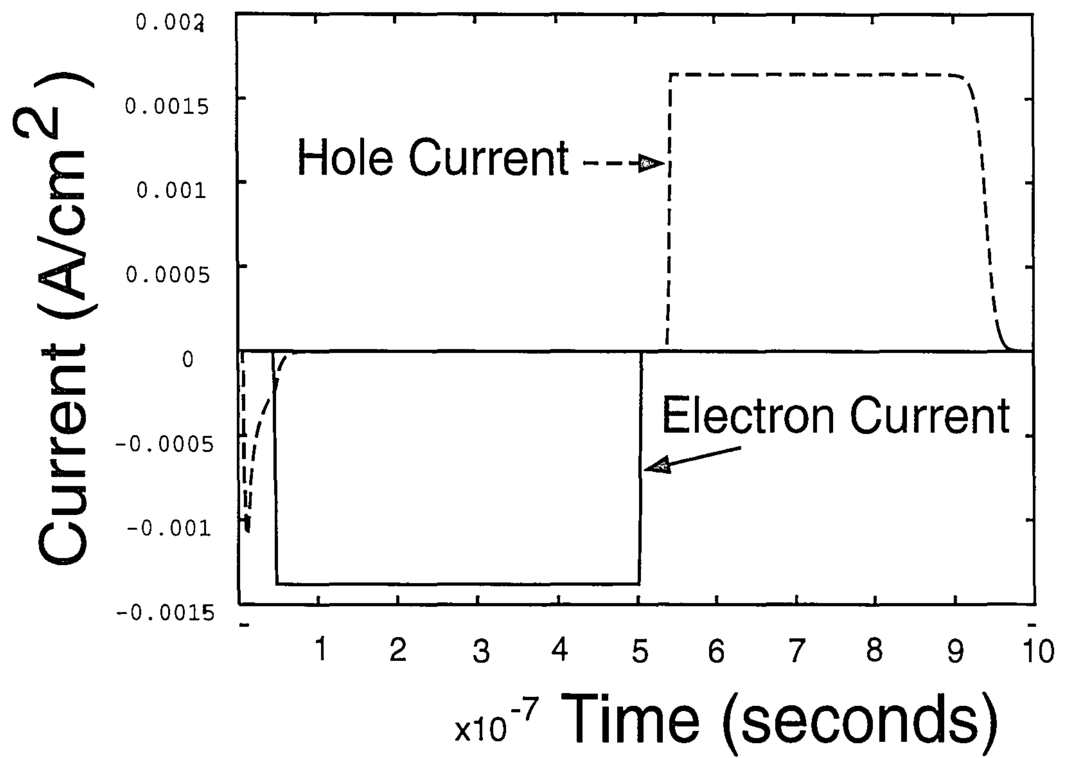

Figure 4.5: Currents at 77 K for the gate voltage of figure 4.1.

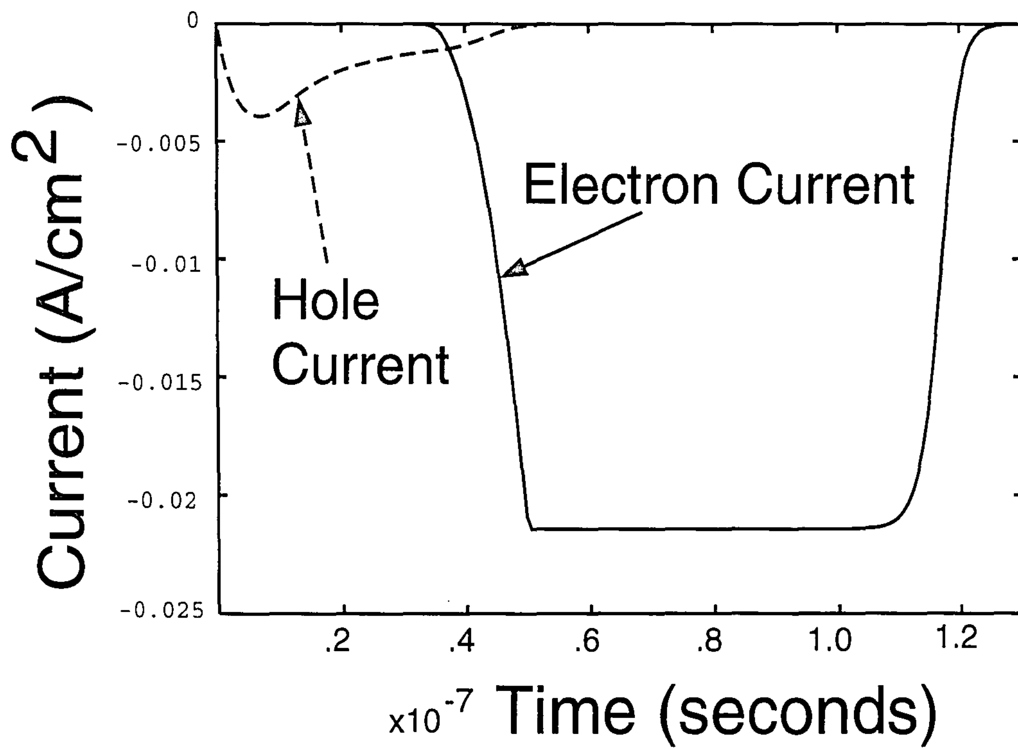

Figure 4.6: Closeup of the rising edge of the waveform shown in figure 4.3

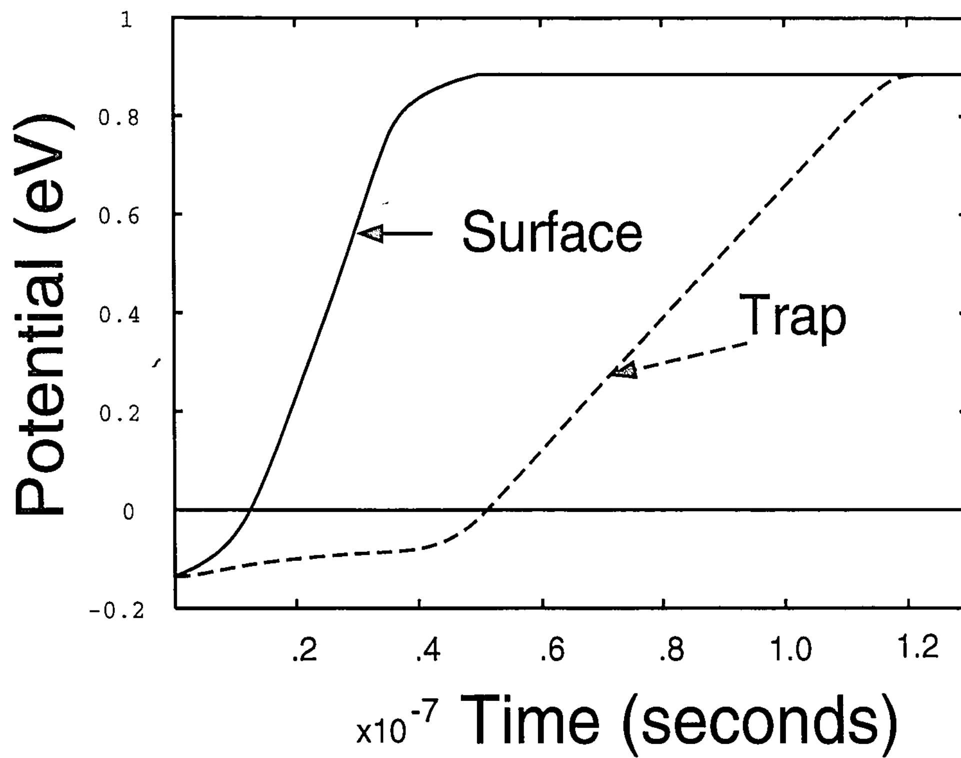

Figure 4.7: Surface and trap potentials for the currents shown in figure 4.6

electron current reaches its maximum value. It stays at this value until the trap potential reaches the threshold value (ψ_t = .79). After this point, the electron current rapidly decreases toward 0.

The falling edge waveforms are shown in figure 4.7 and 4.8. First the electrons

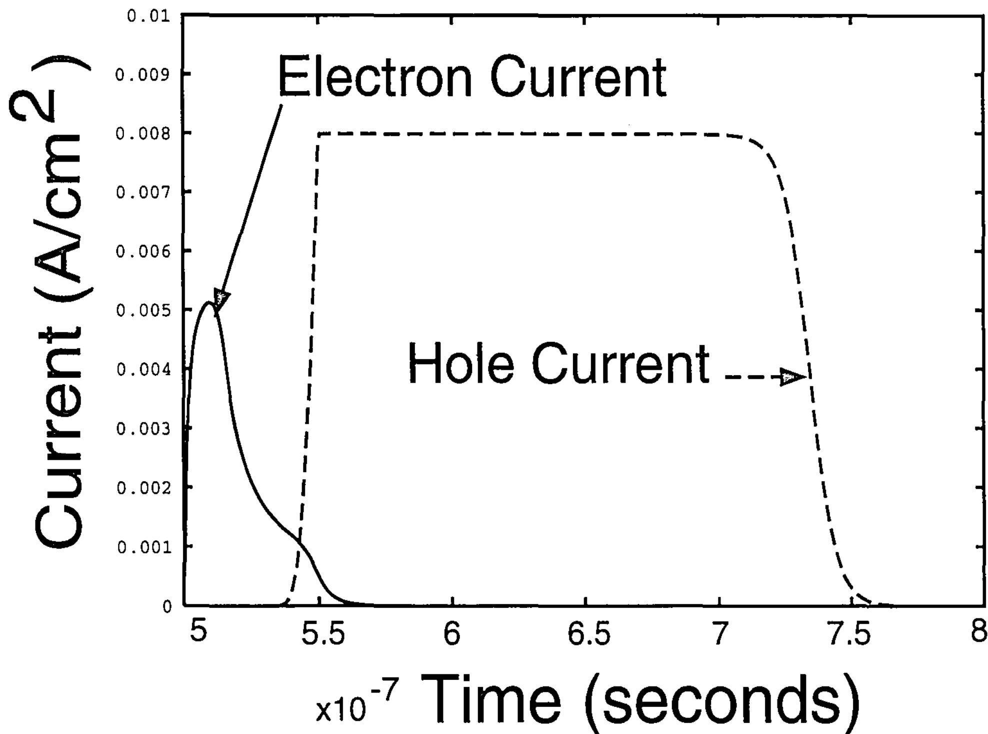

Figure 4.8: Closeup of the falling edge currents of the waveform shown in figure 4.3

emit from the traps, this continues until the trap potential is close to the threshold value. The hole capture starts to increase when the surface potential reaches the flatband voltage. It reaches its maximum value when the trap potential reaches the threshold value and stays there until the trap potential reaches flatband.

One of the assumptions in the formulation of the equations of the two-level pumping experiments is that the current will remain constant independent of the high and low voltage levels as long as the high level is above the threshold voltage

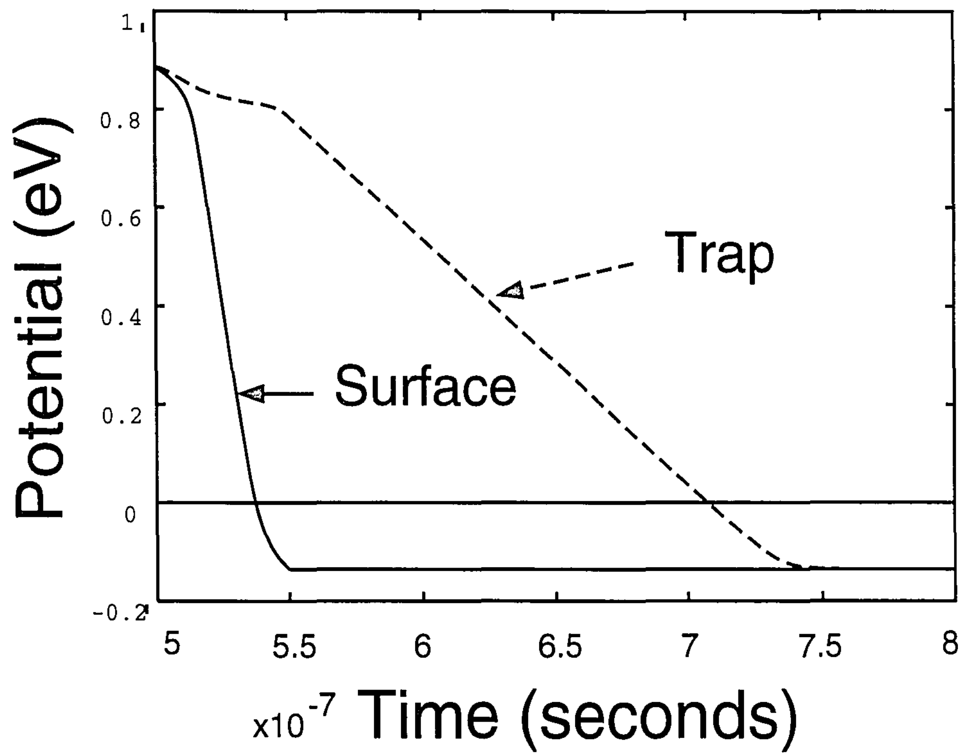

Figure 4.9: Surface and trap potentials for the currents shown in figure 4.8

and the low level is below the flatband voltage. The high and low voltages in the waveform of figure 4.1 were changed from 1.5 and -.5 volts to 2.0 and -1.0 volts respectively. The rise and fall times were also changed to 75 nS, so that $\sqrt{t_{r1}t_{f1}}/\Delta V_1 = \sqrt{t_{r2}t_{f2}}/\Delta V_2$ and the current per cycle should remain the same. The charge per cycle only changed from $1.415nC/cm^2$ to $1.437nC/cm^2$. The waveform of the trap and surface potentials are shown in figure 4.10. The waveform of the

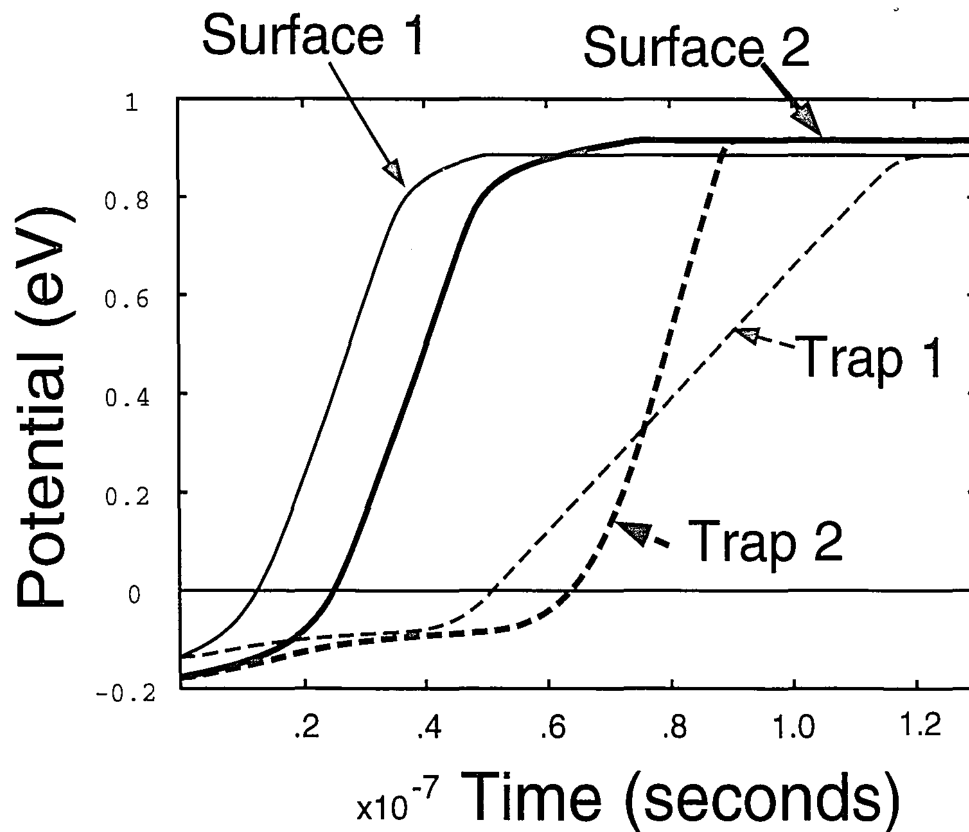

Figure 4.10: ψ_s and ψ_t for an applied waveform of $\Delta V = 2.0V$ and $\Delta V = 3.0V$

currents during the rising edge are shown in figure 4.11. Even though the high and low voltages both changed by .5 V the high and low values for the surface potential hardly changed at all. The trap potential for the waveform with the larger ΔV actually took less time to reach equilibrium than the other one did. This was due

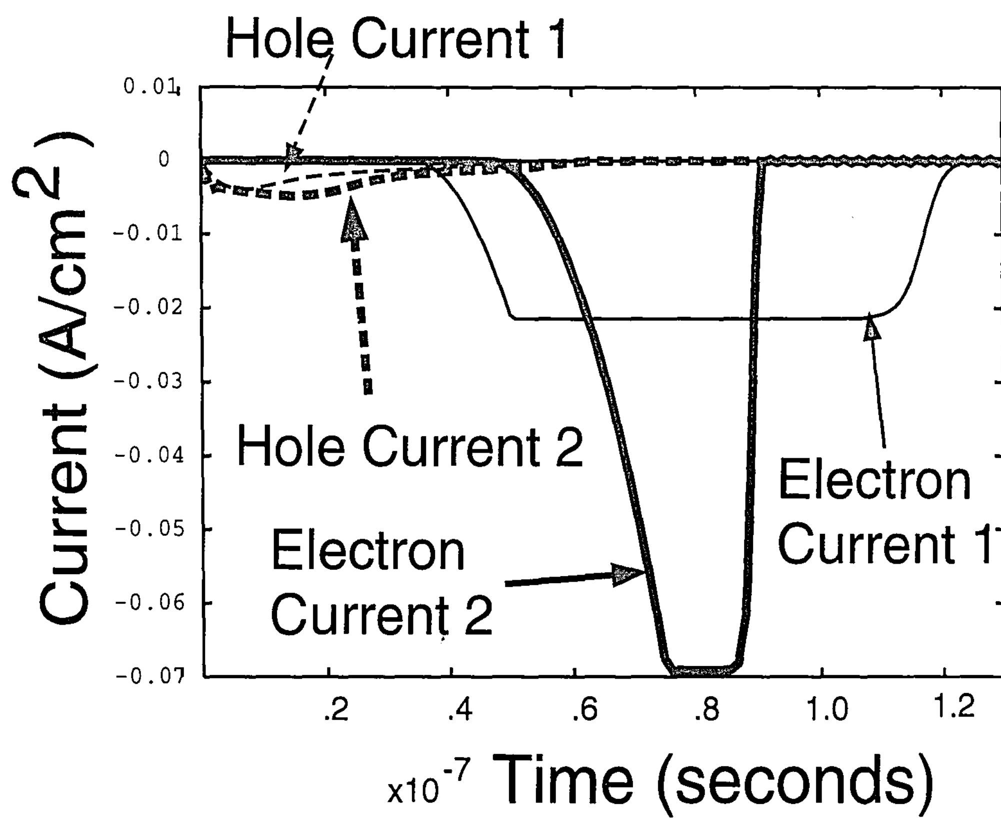

Figure 4.11: Currents corresponding to the potentials shown in figure 4.10

to a greater number of carriers at the surface. As a result the waveforms were very different even though the total current was almost the same.

4.3 Tri-Level

To simulate tri-level charge pumping a waveform similar to figure 2.6 is applied. If the step size is too short the transistor will not reach equilibrium by the end of the step (figure 4.12). The currents will not reach zero before the the gate voltage decreases again (see figure 4.13).

On the other hand, if the step time is increased equilibrium can be reached as figures 4.14 and 4.15 show. (Please note the scale change between the figures.) As figure 4.15 shows the current did reach zero before the gate voltage decreased the second time. The charge per cycle decreased from $1.42nC/cm^2$ to $1.24nC/cm^2$ when the step size was increased. The two-level waveform (the limit when step size approaches zero) produced a charge per cycle of $1.47nC/cm^2$.

4.4 Quantum

When a bulk bias is applied, two main effects occur. First, the curve of surface potential vs. gate voltage changes and there are fewer free carriers. Also the capture cross section changes. With computer simulations we can look at the contribution of these effects. Referring to figure 4.16 we can see that the two curves that use the curve for surface potential assuming zero bulk bias start at the same point, and

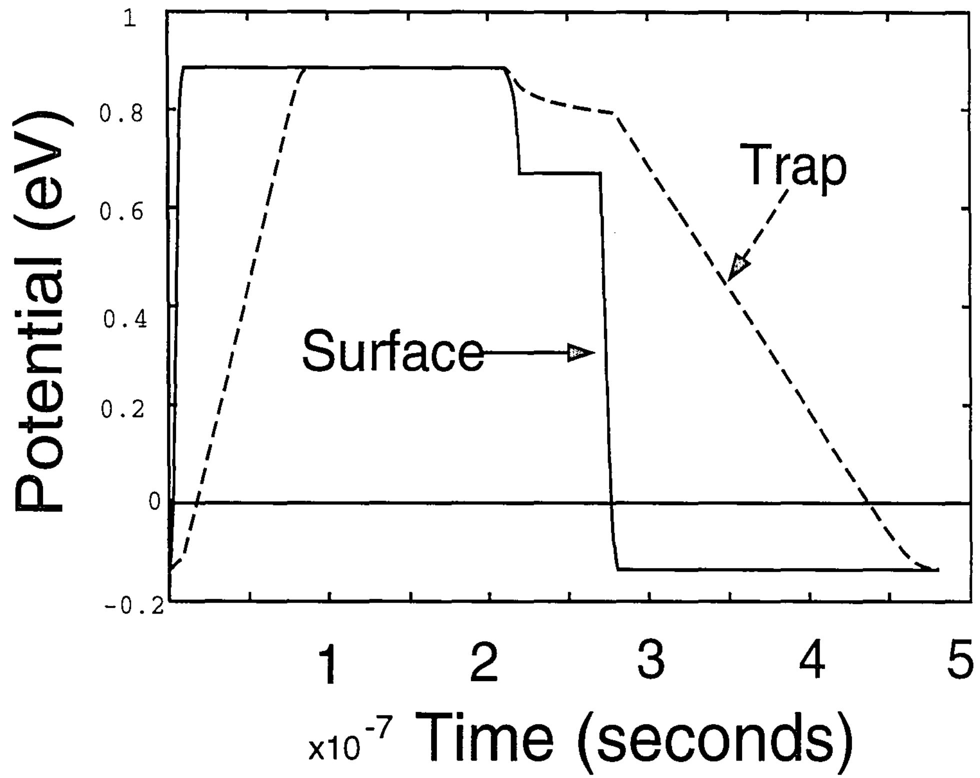

Figure 4.12: ψ_s and ψ_t not at equilibrium with a tri-level waveform applied to this device.

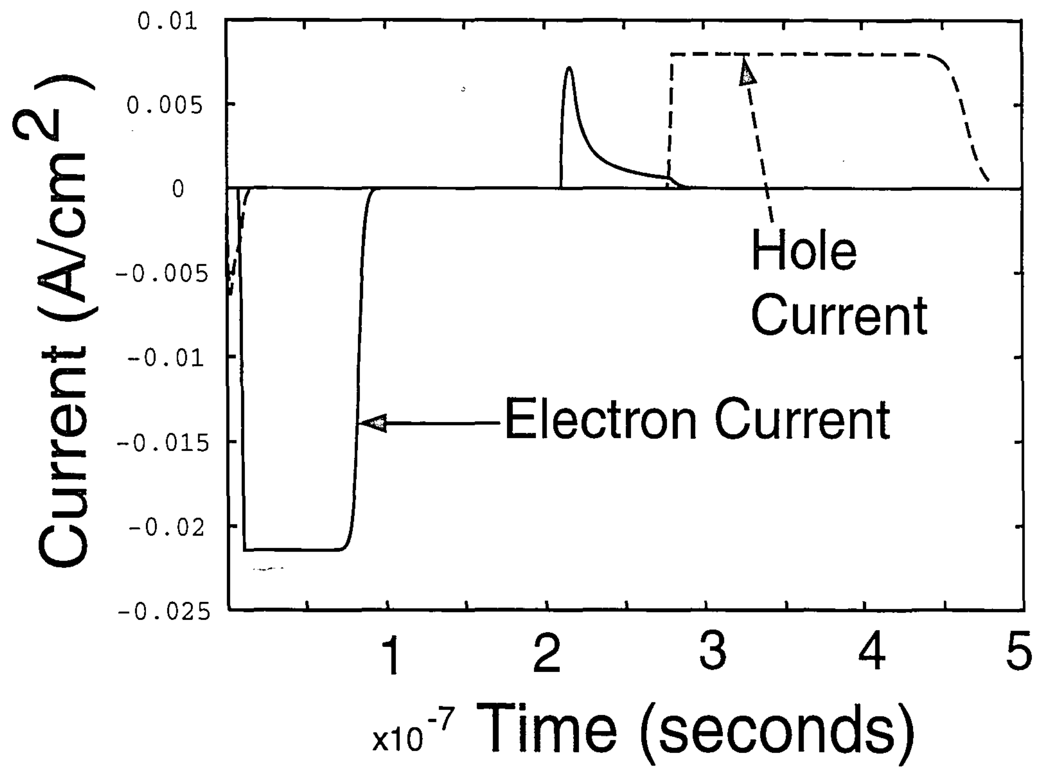

Figure 4.13: Currents not at equilibrium for the applied tri-level waveform, these currents correspond to the potentials shown in figure 4.12.

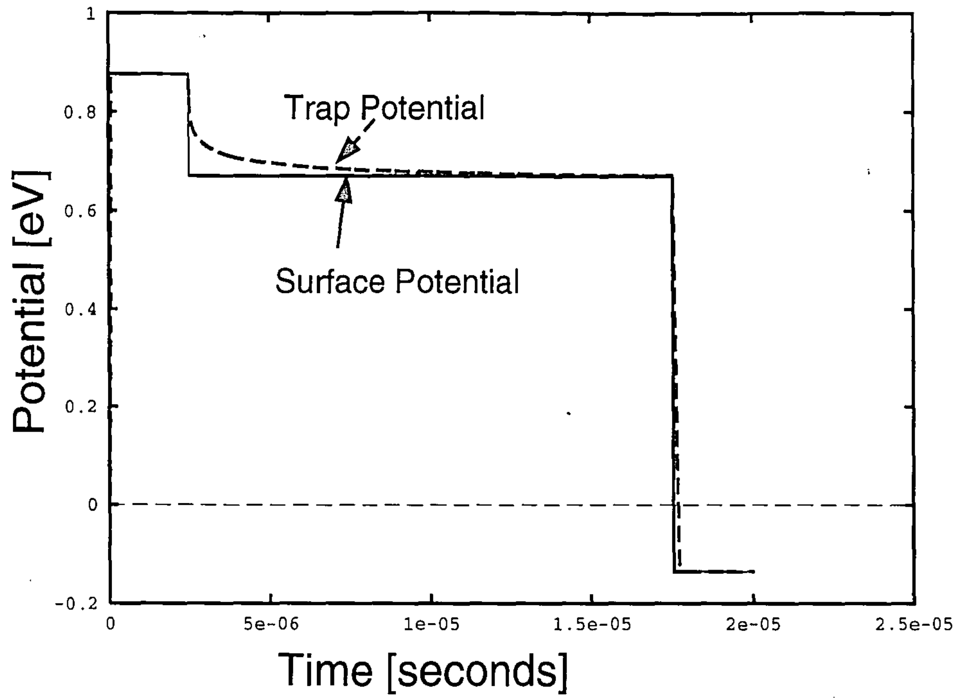

Figure 4.14: ψ_s and ψ_t at equilibrium for the applied tri-level waveform.

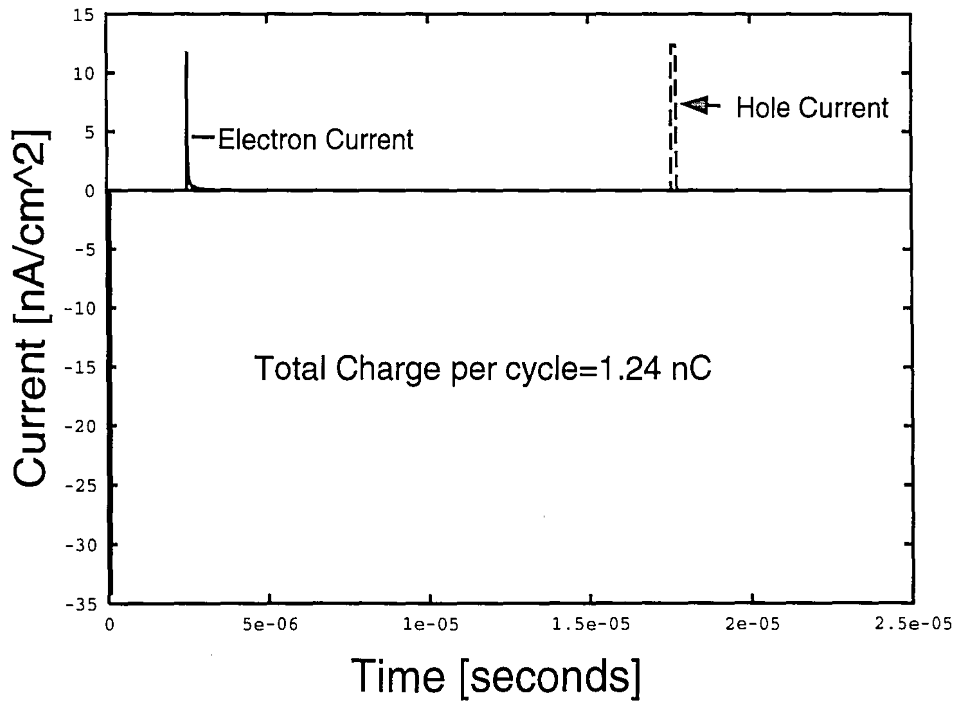

Figure 4.15: Currents at equilibrium

those that assume a $-2V$ bulk bias start at a different point. All the curves end up at the same point. This is because the V_g curves are equivalent for negative gate voltages independent of the bulk bias. After a short while, the trap potentials for the 2 cases corresponding to the larger capture cross sections come together and the other two curves also come together. This proves that once the gate voltages becomes below the threshold value, the trap potential is determined by the emission rates, which are determined by the capture cross sections.

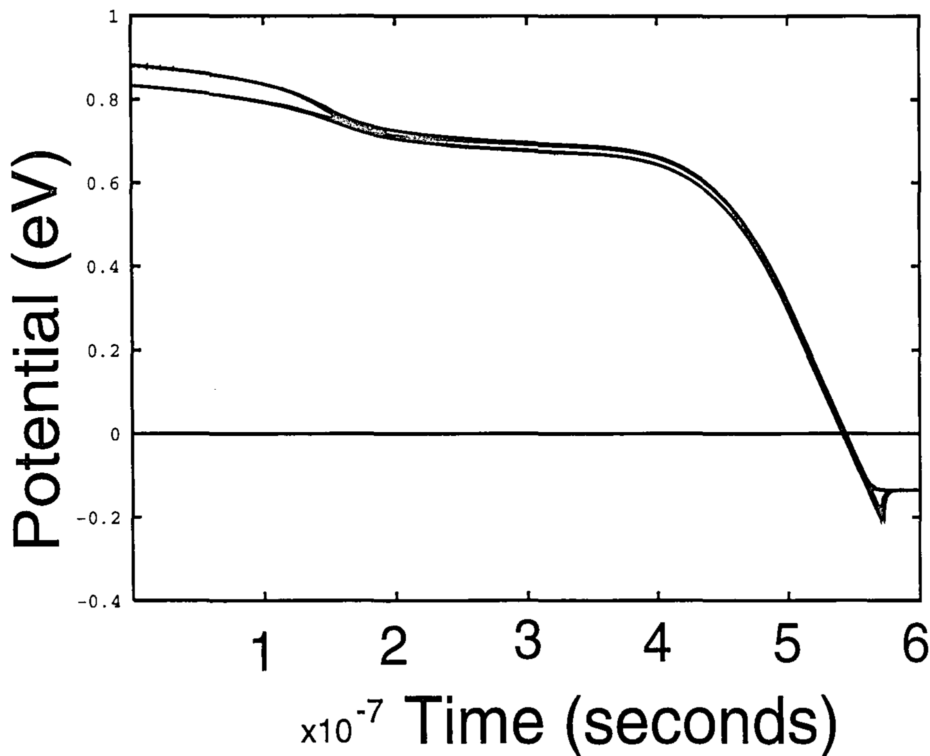

Figure 4.16: Trap potential for the various combinations of two different capture cross sections and two different bulk biases

Chapter 5

Computer Simulation of Charge Pumping Experiments

5.1 Introduction

The overall currents were compared to theoretical as well as to devices fabricated in the lab. Table 4.1 contains the constants that were used for these simulations, except where noted. Unlike the previous sections these results can be compared with actual devices and not just theoretical results.

The devices used in the experiments were fabricated in the microelectronics laboratory following Lehigh University's standard processing sequence shown in appendix B. The tests were carried on with the experimental setup shown in appendix C.

5.2 Two-Level Results

The graph of Q_{CP} vs. log of frequency (shown in figure 5.1) for the sawtooth pulse agrees well with the expected results. When the frequency is varied with a

square waveform applied the charge per cycle remains constant as figure 5.2 shows.

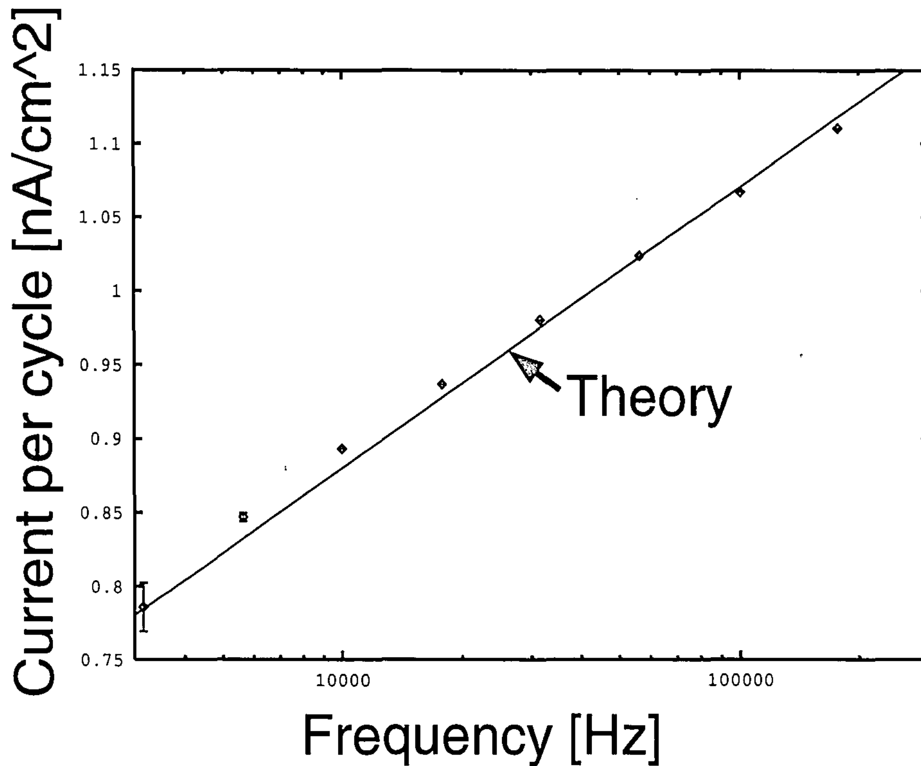

Figure 5.1: Q_{CP} as a function of frequency for sawtooth pulse ($\alpha = .5$).

The graph of Q_{CP} for different base levels in shown in figure 5.3. The Flatband voltage for this simulation was 0 volts. This is slightly higher than the location where the current is at half of its maximum value. The threshold voltage (where $\psi_s = 2\psi_f$) is at .97 volts. The other location corresponding to half the maximum current is when $V_L = -1$, since $\Delta V = 2$ the estimated threshold voltage from the graph is $\Delta V_G + V_L = 1$.

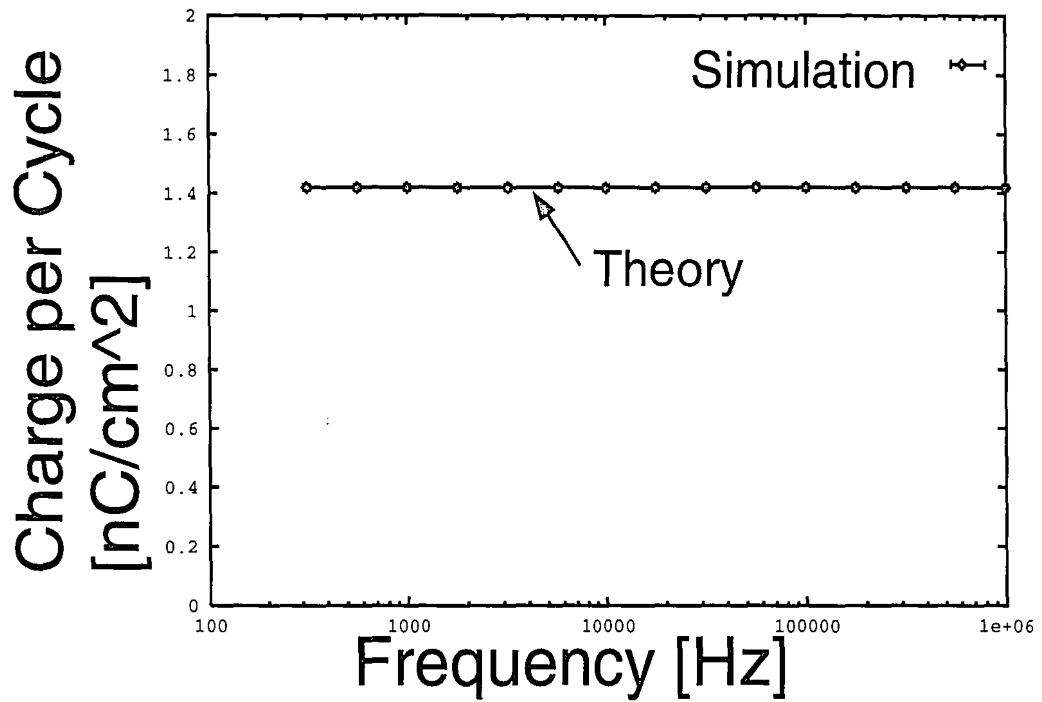

Figure 5.2: Q_{CP} as a function of frequency for a square pulse

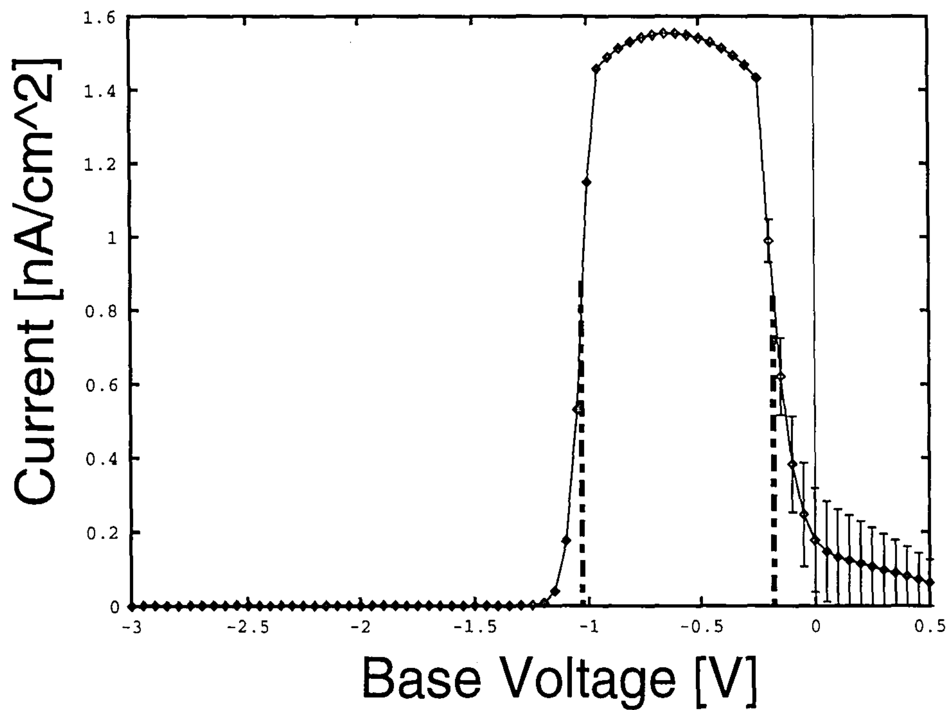

Figure 5.3: Q_{CP} for various base levels

5.3 Tri-level

By graphing Q_{CP} for different step sizes and various step voltages the different parameters can be extracted. As shown in figure 5.4 the program produced reasonable results. The curves came close to one another for short step times and also saturate for longer step times. The curves that did not saturate have emission times that are longer than the time period of the simulations.

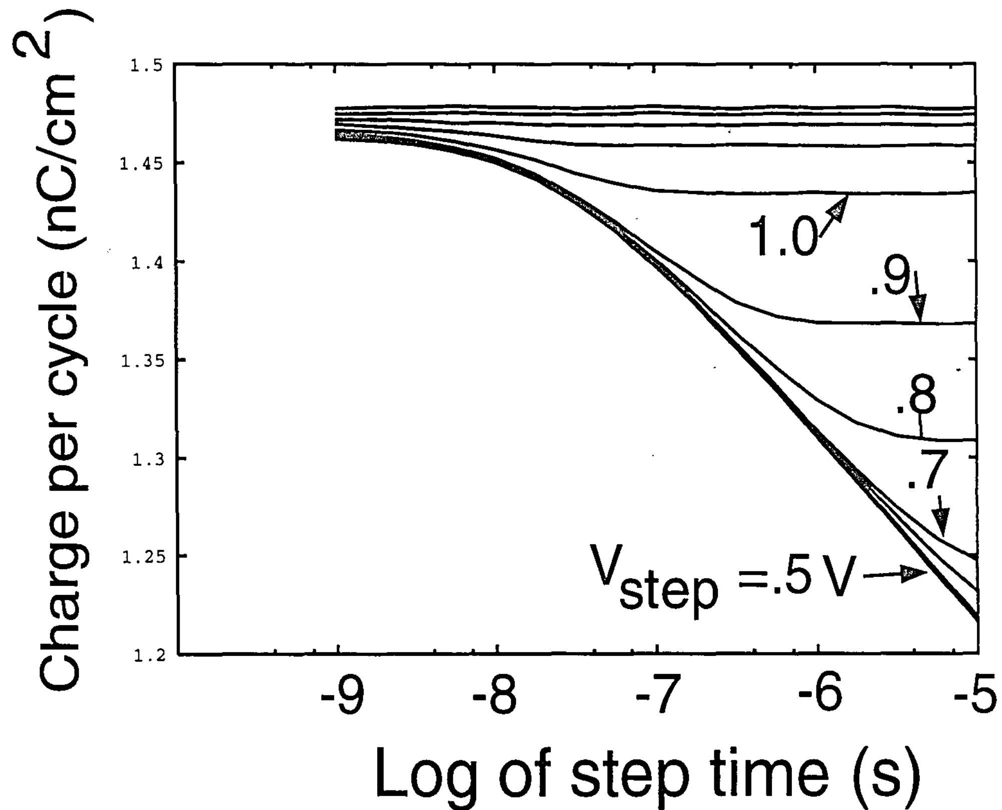

Figure 5.4: Graph of Q_{CP} vs. step size for different step voltages

The emission time for electrons, τ_e can be estimated from the breakpoint of the curves. If the voltage step had been on the leading edge, then τ_h would be the breakpoint. Equations 2.33 and 2.34 can be used to find $E(t)$ and σ_n. Since σ_n was

one of the inputs to the program, the value used in the program can be checked with the value calculated from the graph. A plot of the emission times vs. trap level is shown in figure 5.5. The intercept of the lines is at the pinning level. This again compares well with the theoretical value. Tri-level experiments find D_{it} as

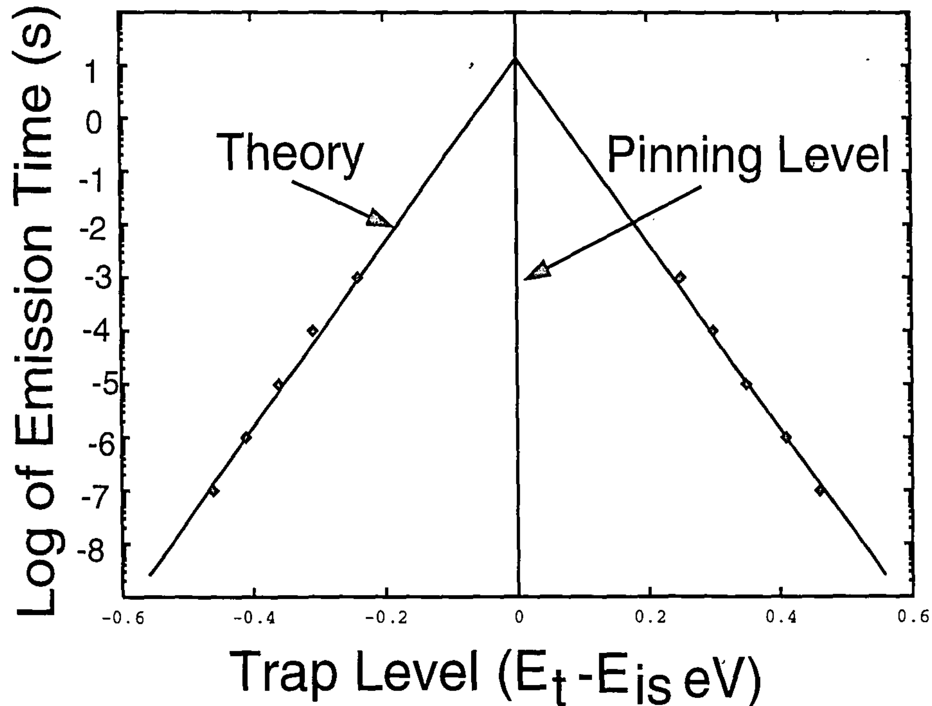

Figure 5.5: Graph of emission times

a function of trap level by using equation 2.43. As figure 5.6 shows D_{it} was fairly constant over the entire range of energies.

5.4 Quantization

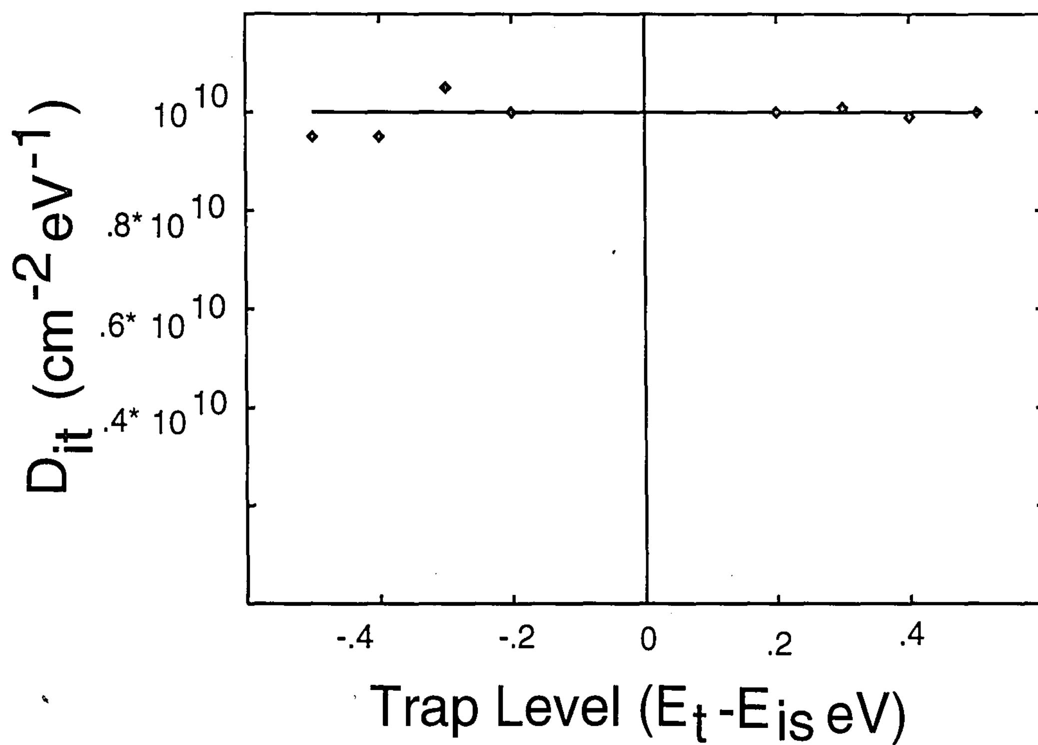

Figure 5.6: Graph of D_{it} as a function of trap level

By applying equation 2.50, the quantization levels can be simulated. As shown in figure 5.7 the current varies depending on V_{SB}. As the step time increases, the the currents become equal, which means that the same trap level is probed in each case. The curves do not have the same values for small times because the bulk bias changes the threshold voltage, which affects the current for the two-level pulses and the short step times. The values for the breakpoints are similar to the experimental data taken by Siergiej[1].

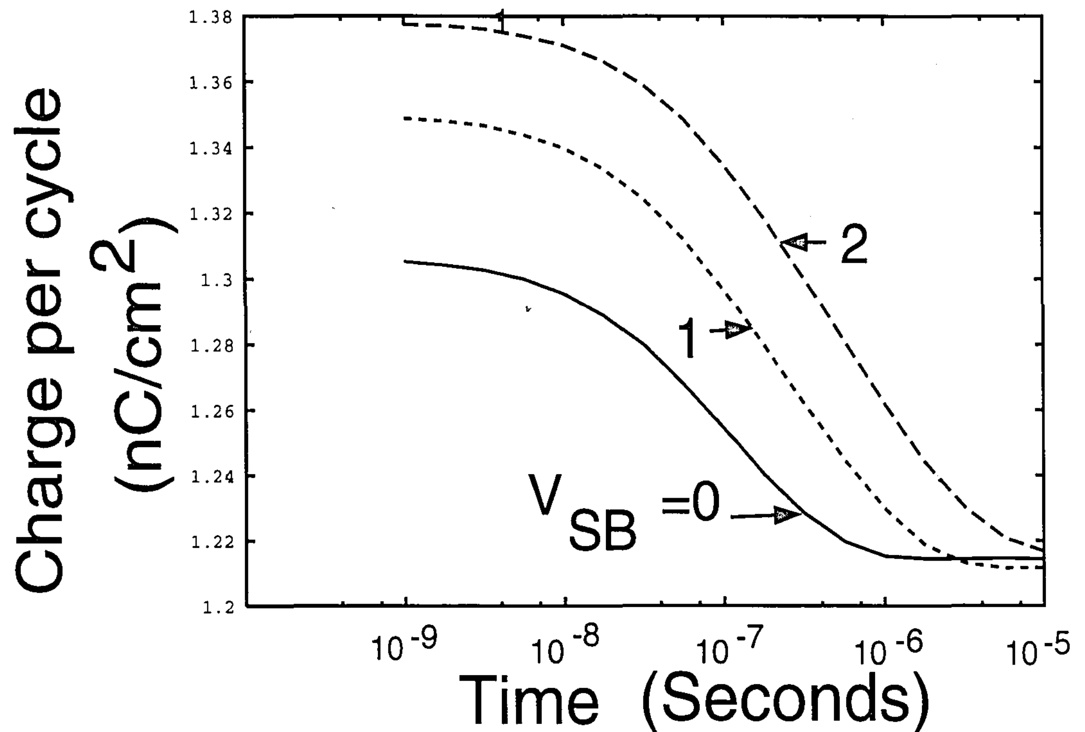

Figure 5.7: Charge per cycle for differing values of bulk biasing

5.5 Comparison to Fabricated Devices

Once the correct operation of the program was confirmed by the simulations shown above, it was compared to experimental data from devices fabricated in the processing lab. The devices were manufactured following the NMOS processing sequence shown in appendix B.

Figure 5.8 shows the results of the simulations compared to the experimental results for different base voltages. The simulated results are close to the experimental results. The user supplied constants were set to try to approximate the values of the device used in the experiment.

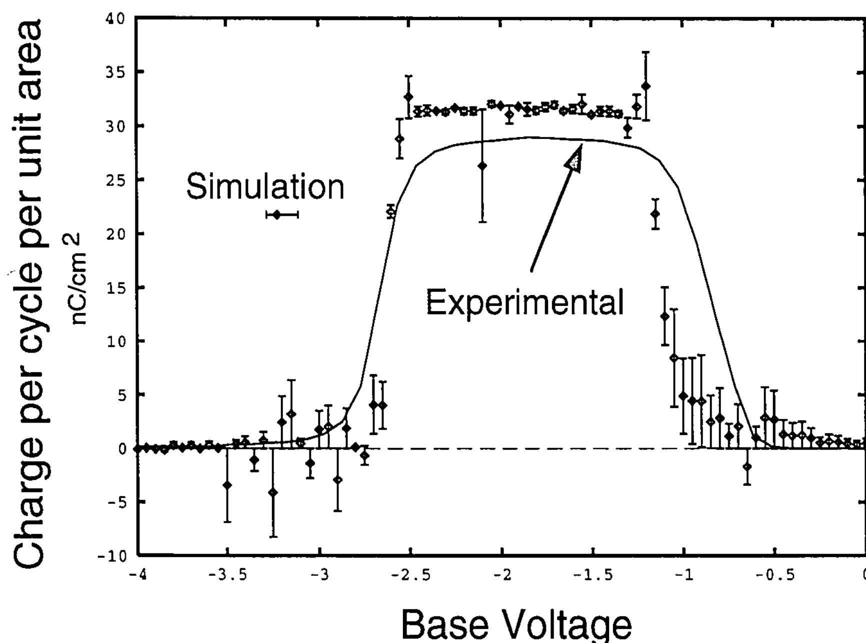

Figure 5.8: Simulation results compared to experimental data

Since each processing run is slightly different, the flatband voltage and bulk doping density had to be determined experimentally. These parameters were obtained from FLUTE (Friendly Lehigh University Transistor Extraction program). This program was developed by Dr. Thomas Krutsick and Dr. Richard Booth. The tests were carried out by FIDDLER (Friendly Interactive Data Dowser for Learned

Extractors by Richard). Please see Appendix C for a more detailed description of the test setup and these programs.

5.6 Conclusions

All the tests run both those shown here as well as other tests, confirmed the proper execution of the program. It produces results that are close to what is expected theoretically. The hole and electron currents were normally off by less than .1 % from each other.

	V_{FB}	V_T
Actual	0	.97
Simulation	-.2	.9

Table 5.1: Threshold and flatband Voltages found by varying the base level compared to theory

Method	$\overline{D_{IT}}$	$\sqrt{\sigma_n \sigma_p}$
Actual	10^{10}	10^{-17}
Sawtooth	$9 * 10^{9}$	$3 * 10^{-18}$
Vary Base	$1.1 * 10^{10}$	
Tri-level	10^{10}	$1.1 * 10^{-17}$

Table 5.2: Summary of experiments for D_{it} and capture cross sections.

The simulations that incorporated the quantization effects produced results that

were close to the theory. The experiments that Siergiej [1] performed were simulated. The simulation program was also close to the actual experimental results. There

Substrate Bias (V)	Emission Time of Simulation (S)	$\ln(\frac{\tau_e}{\tau_e \mid V_{SB}=0})$		
0	$3 * 10^{-7}$	Simulation	Experiment [1]	Theory
1	$2 * 10^{-6}$	1.9	2.2	2.85
2	$6 * 10^{-6}$	3.00	3.67	3.67

Table 5.3: Summary of simulation of quantization effects

are several factors that may explain the slight differences. The oxide thickness was not measured on the actual device that was tested. Instead control wafers were measured, and the device wafer was assumed to have similar thickness. Also, the exact capture cross section of the sample was not known. The simulated capture cross sections were both set equal to $1 * 10^{16}$. Fiddler assumes that $\sqrt{\sigma_n \sigma_p} = 1 * 10^{16}$. The simulation assumed a constant $D_{it}(E)$ which may not have been the case. In spite of these possible sources of errors, the simulation results were close to the FLUTE numbers as well as the experimental results. Table 5.4 provides a summary of the results.

Method	$\overline{D_{IT}}$	V_{FB}	V_T
FLUTE		$-.098$	.00335
Experimental	$2.63 * 10^{11}$	$-.853$	$-.164$
Simulation	$2.33 * 10^{11}$	-1.3	.05

Table 5.4: Comparison of experimental data to simulations with square wave pulses

Chapter 6

Conclusions

6.1 Accomplishments

The simulations produced results in agreement with the theories for the different cases tried. It also was in agreement with actual experimental data. A theory is worthless if it does not explain what happens in real experiments.

The current waveforms allow further understanding of the operation of charge pumping. Unlike the actual experiments, these waveforms can be analyzed. It could make a good teaching tool to explain how the various components are related to one another.

These simulations serve as further proof of Siergiej's theory of quantization layers. For the first time, these effects have been included in a computer simulation program. The assumption that $\sigma_n(2D)$ can be treated as a constant was confirmed.

6.2 Suggestions for Future Work

The computer simulations required a long time to run. The algorithm could

be studied and possibly improved to increase the speed. Changing the code to produce acceptable results was done by trial and error instead of theoretical studies of numerical techniques.

Another simple study would be to check operations of p-channel semiconductors. This would require very few changes to the program. These simulations were not carried out because of the extra time required. The simulations could be easily compared to new devices fabricated in the lab. If new devices are fabricated they could be designed to increase the quantization effects by increasing the doping densities.

The simulations could be improved by adding the effects of near-oxide interface traps. This would increase the number of conditions where this simulator will produce correct results. Since the geometric component was not included, the simulations are only valid for transistors of high width to length ratios. The recent work of Van den bosch, et al. [29] may make it fairly easy to include these effects. It would also be interesting to view the current waveforms associated with both of these effects. Instead of just the hole and electron currents, the current into the near-interface oxide traps and the geometric current would also plotted.

The program assumes a constant density of traps throughout the energy gap. It has been shown that this is probably not a good assumption [6, 30]. Also, the capture cross sections are assumed to be independent of energy. The approach could be changed to include these two effects.

As it is currently written a uniform doping density is assumed. Actual devices don not have a uniform doping density. The effect of a non-uniform doping density could be included. Another effect that could be considered would be the incomplete ionization of the dopants. This would be harder to incorporate since the amount that is ionized depends on the surface potential, so it would have to be recalculated at each point in time. This would allow accurate results to be obtained even at low temperatures and high doping densities.

Currently the user must find τ_e or τ_h by eye balling the breakpoint. The computer could be set to automatically find this value. This would make the results more uniform and less subject to human interpretation.

Finally, the program could be made easier to use. In order to change the parameters, the user would have to change the actual program and recompile it. If the user accidently changes something they are not supposed to the entire program could be destroyed. Either an interactive interface or a separate file for the constants could be used.

In the area of measurements, the Sun workstations could be set up to control the equipment. This would allow the data between experiments and simulations to be compared more easily. One of the lab's workstations has an IEEE card in it to connect to the IEEE Bus. The auto prober could be employed to step across the wafer to measure different devices and compare them to one another.

Dr. Richard Siergiej's low temperature setup[31] could be used to study the low temperature effects. This would allow operation at temperatures down to liquid Helium. The low temperature would increase the quantization effects.

References

[1] Richard Siergiej. *Quantization Effects on Interface Modeling and Techniques to Characterize Highly Doped Oxy-Nitride and Pure Oxide Silicon Field Effect Transistors.* PhD thesis, Lehigh University, 1992.

[2] J.S. Brugler and P.G.A. Jespers. "Charge Pumping in MOS Devices". *IEEE Trans. Electron Devices*, ED-16(3):297–302, Mar. 1969.

[3] G. Groeseneken, H.E. Maes, N. Beltran, R.F. De Keersmaecker. "The Energy Distribution of Si/SiO_2 Interface States Measured in Small Size MOSFET's Using the Charge Pumping Technique". In *Insulating Films on Semiconductors*, 1983.

[4] W.L. Tseng. "A New Charge Pumping Method of Measuring Si-SiO_2 Interface States". *J. Appl. Phys.*, 62(2):591–599, Jul. 1987.

[5] L.M. Terman. "An Investigation of Surface States at a Silicon/Silicon Oxide Interface Employing Metal-Oxide-Silicon Diodes". *Solid State Electron.*, 5:285–299, 1962.

[6] P.V. Gray and D.M. Brown. "Density of SiO_2-Si Interface States". *Appl. Phys. Lett.*, 8(2):31–33, January 1966.

[7] C.N. Berglund. "Surface States at Steam-Grown Silicon-Silicon Dioxide Interfaces". *IEEE Trans. Electron Devices*, ED-13(10):701–705, Oct. 1966.

[8] R. Castagné and A. Vapaille. "Description of the SiO_2-Si Interface Properties by means of Very Low Frequency MOS Capacitance Measurements". *Surf. Sci.*, 28:157–193, 1971.

[9] M. Kuhn. "A Quasi-Static Technique for MOS C-V and Surface State Measurements". *Solid-State Elect.*, 13:873–885, 1970.

[10] E.H.Nicollian and A.Goetzberger. "The Si-SiO_2 Interface - Electrical Properties as Determined by the Metal-Insulator-Silicon Conductance Technique". *Bell System Technical Journal*, pages 1055–1133, Jul.-Aug. 1967.

[11] E.H. Nicollian and A. Goetzberger. "MOS Conductance Technique for Measuring Surface State Parameters". *Appl. Phys. Letts.*, 7(8):216–219, October 1965.

[12] N.M. Johnson, D.J. Bartelink, and M. Schulz. "Transient Capacitance Measurements of Electronic States at the SiO_2-Si Interface". In S.T. Pantelides, editor, *Physics of SiO_2*, pages 421–427. 1978.

[13] E. Klausmann. "Si/SiO_2 Properties Investigated by the CC-DLTS Method". In *INFOS*, pages 169–173, 1981.

[14] Y. Nishi. "Study of Silicon-Silicon Dioxide Structure by Electron Spin Resonance I". *Jap. J. of Appl. Phys.*, 10(1):52–62, January 1971.

[15] A.S. Grove. *Physics and Technology of Semiconductor Devices.* John Wiley and Sons, New York, 1967.

[16] G. Ghibaudo. "New Method for the Extraction of MOSFET Parameters". *Electronics Letters*, 24(9):543–545, Apr. 1988.

[17] R.A. Wachnik. "The Use of Charge Pumping to Characterize Generation by Interface Traps". *IEEE Trans. Electron Devices*, ED-33(7):1054–1061, July 1986.

[18] H.E. Maes and G. Groeseneken. "Determination of Spatial Surface State Density Distribution in MOS and SIMOS Transistors After Channel Hot Electron Injection". *Electronics Lett.*, 18(9):371–374, April 1982.

[19] F.L. Schuermeyer, C.R. Young, and W.G. Sutton. "Charge-Pumping Investigations on MNOS Structures". *IEEE Trans. on Electron Devices*, ED-24(5):552–559, May 1977.

[20] H.E. Maes and S.H. Usmani. "Charge Pumping Measurements on Stepped-Gate Metal-Nitride-Oxide-Silicon Memory Transistors". *J. Appl. Phys.*, 53(10):7106–7108, October 1982.

[21] Gerard Ghibaudo and Nelson S. Saks. A time domain analysis of the charge pumping current. *Journal of Applied Physics*, 64(9):4751–4754, November 1988.

[22] W.Shockley and W.T.Read, Jr. "Statistics of the Recombinations of Holes and Electrons". *Physical Review*, 87(5):835–842, Sep. 1952.

[23] R.N. Hall. "Electron-Hole Recombination in Germanium". *Phys. Rev.*, 87:387, 1952.

[24] S. M. Sze. *Physics of Semiconductor Devices.* John Wiley & Sons, 2nd edition, 1981.

[25] Nicolas Beltran Guido Groeseneken, Herman E. Maes and Roger F. De Keersmecker. A reliable approach to charge-pumping measurements in mos transistors. *IEEE Transactions On Electron Devices*, ED-31(1):42–53, January 1984.

[26] R.E. Paulsen, R.R. Siergiej, M.L. French, and M.H. White. "Observation of Near-Interface Oxide Traps With the Charge Pumping Technique". *Electron Device Letters*, 13(12), December 1992.

[27] Ron Paulsen. The study of near-interface oxide traps and tunneling in mos devices with the charge pumping technique. Master's thesis, Lehigh University, May 1993.

[28] J. G. Simmons and L. S. Wei. Theory of dynamic charge current and capacitance characteristics in mis systems containing distibuted surface traps. *Solid-State Electronics*, 16:53–66, 1973.

[29] Guido Groeseneken Geert Van den bosch and Herman E. Maes. On the geometric component of charge-pumping current in mosfet's. *IEEE Electron Device Letters*, 14(3):107–109, March 1993.

[30] M.R. Boudry. "Theoretical Origins of N_{ss} Peaks Observed in Gray-Brown MOS Studies". *Appl. Phys. Lett.*, 22(10):530–531, May 1973.

[31] Richard Robert Anthony Siergiej. An automated test station for semiconductor device evaluation at cyrogenic temperatures. Master's thesis, Lehigh University, May 1987.

[32] Ricard S. Muller and Theodore I. Kamins. *Device Electronics for Integrated Circuits.* John Wiley and Sons, 2 edition, 1986.

[33] Richard C. Jaeger and Fritz H. Gaensslen. Simulation of Impurity Freezeout Through Numerical Solution of Poisson's Equation with Application to MOS Device Behavior. *IEEE Transaction on Electron Devices*, ED-27(5):914–920, May 1980.

[34] Fritz H. Gaensslen and Richard C. Jaeger. Temperature Dependent Threshold Behavior of Depletion Mode MOSFETs. *Solid-State Electronics*, 22:423–430, 1979.

[35] R.R.A. Siergiej. *Quantization Effects on Interface Trap Modeling and Techniques to Characterize Highly Doped Oxy-Nitride and Pure Oxide Silicon Field Effect Transistors.* PhD thesis, Lehigh University, May 1992.

[36] R.V.H. Booth. *Simulation and Measurement of Hot-Carrier Injection and Degradation in Short Channel MOS Transistors.* PhD thesis, Lehigh University, June 1989.

[37] S. Yoon and M.H. White. "Study of Thin Gate Oxides grown in an Ultra-Dry/Clean Triple-Wall Oxidation Furnace System". *J. of Electronic Materials*, 19(5):487–493, 1990.

[38] T.K. Krutsick. *A Study of Carrier Mobility in Quantized MOSFET Inversion Layers.* Doctoral Dissertation, Lehigh University, June 1988.

[39] T.J. Krutsick, M.H. White, H.-S. Wong, and R.V.H. Booth. "An Improved Method of MOSFET Modeling and Parameter Extraction". *IEEE Trans. Electron Devices*, ED-34(8):1676–1679, Aug. 1987.

Appendix A

Properties of Si

A.1 Introduction

In order to understand how charge pumping varies under different operating conditions and doping levels, it is necessary to look into the physics of the semiconductor used in the experiments. The following sections develop the equations for the band gap, intrinsic carrier concentration, and the surface potential vs. gate voltage. These effects are included in the program to enable correct results to be obtained over a wide range of conditions.

A.2 Band Gap

All semiconductors have bands where electrons are allowed to exist and a region between the valance and conduction bands where they can not. The valance band, E_v, ends at the lower edge of the energy gap. The conduction band, E_c, is the upper edge of the band gap. The energy gap, E_g, is the difference between the two levels. It can be expressed as[24]

$$E_{go} = 1.170 - \frac{4.73 * 10^{-4} T^2}{T + 636} \tag{A.1}$$

At room temperature, $E_{go} \approx 1.12$ (eV).

If high enough dopants are present, the band gap will become narrower because of the stored electrostatic energy of the majority-minority carrier pairs. The band gap reduction is given by[24]

$$\Delta E_g = \frac{3q^2}{16\pi\epsilon_s}\frac{q^2 N_B}{\epsilon_s kT} \tag{A.2}$$

where N_B is the bulk doping density. The final value for the bandgap will be

$$E_g = E_{go} - \Delta E_g. \tag{A.3}$$

A.3 Carrier Concentration

The intrinsic carrier concentration, n_i, is a strong function of temperature.[32]

$$n_i = \sqrt{N_c N_v} e^{-E_g/2kT} \tag{A.4}$$

where N_c and N_v, the effective densities of states at the edges of the conduction and valence bands, respectively, are given by

$$N_c = 2\left(\frac{2\pi m_n^* kT}{h^2}\right)^{2/3} \tag{A.5}$$

$$N_v = 2\left(\frac{2\pi m_p^* kT}{h^2}\right)^{2/3} \tag{A.6}$$

where m_n^* and m_p^* are the effective masses of electrons and holes. The electron and hole densities in the bulk are related to the intrinsic level as follows:

$$n_o p_o = n_i^2 \tag{A.7}$$

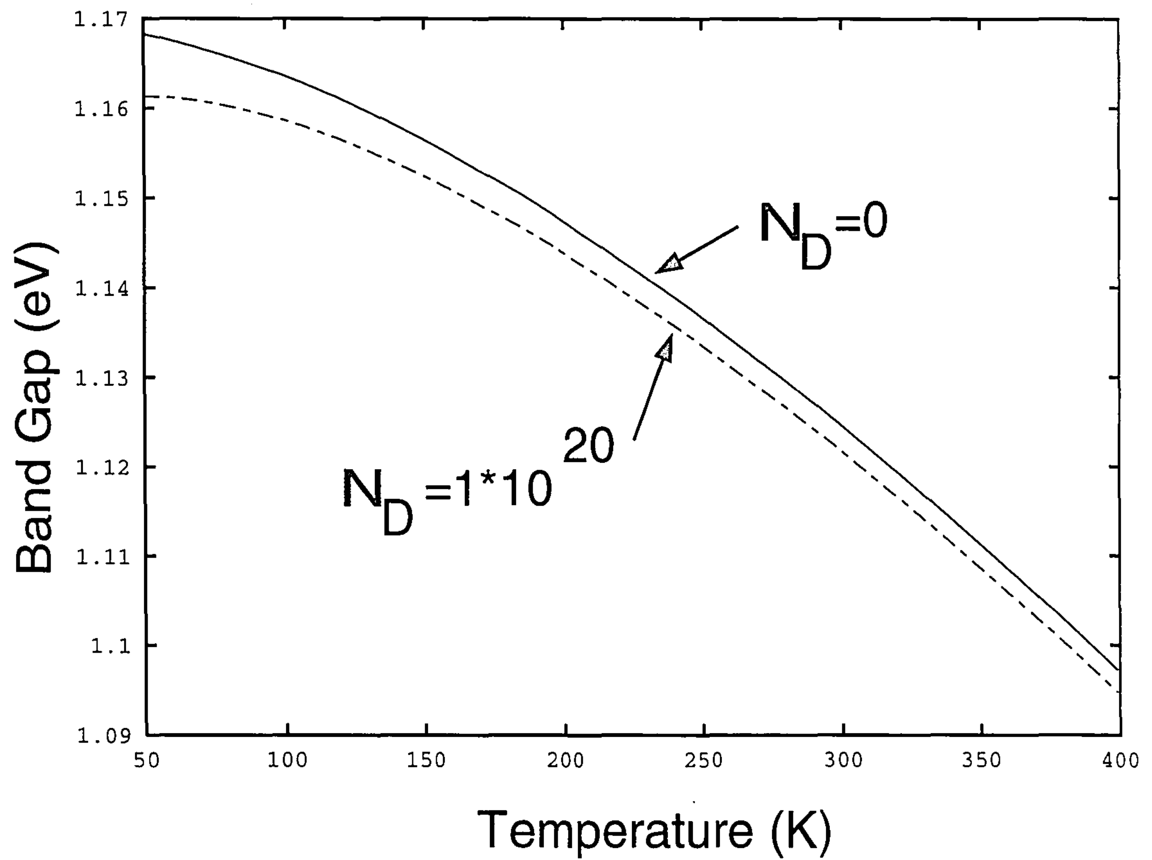

Figure A.1: Band Gap as a function of temperature for different doping levels

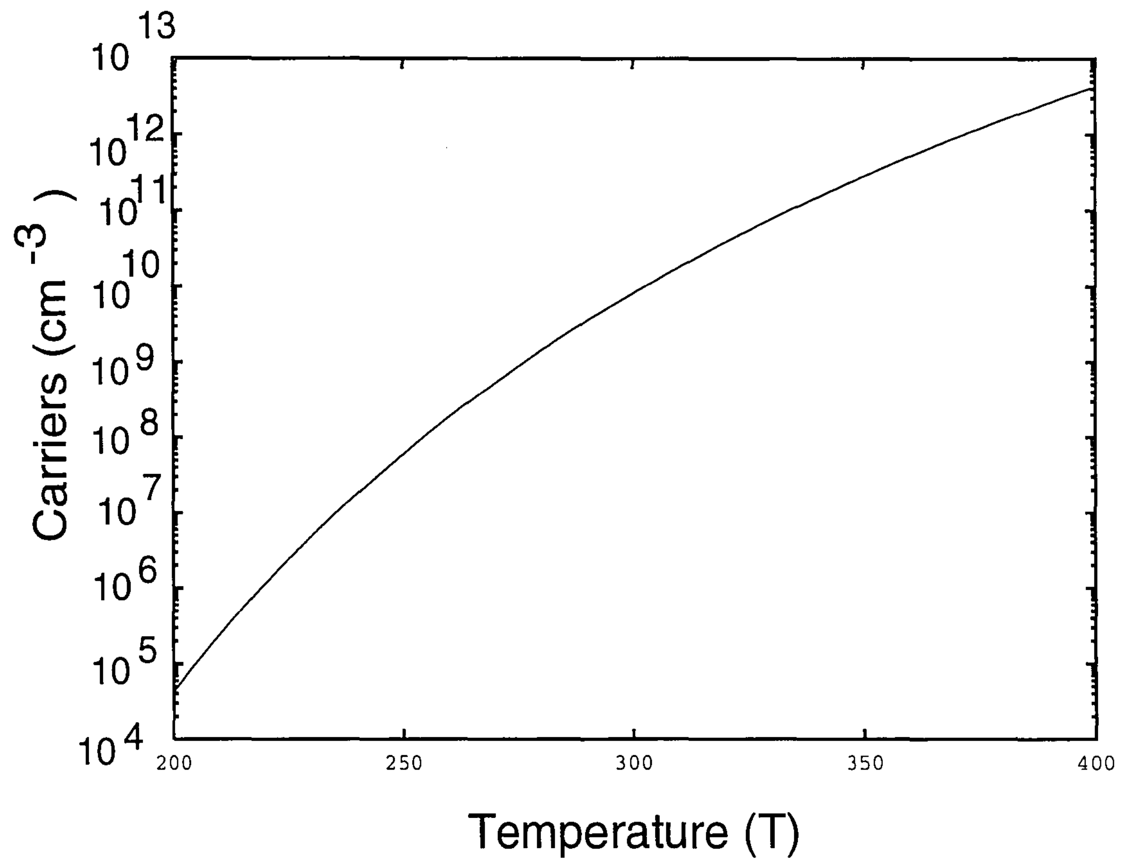

Figure A.2: n_i as a function of temperature

If a bulk bias is applied the concentration of free carriers will decrease.

$$n_o p_o = n_i^2 e^{-qV_{SB}/kT} \tag{A.8}$$

In this study, it is assumed that there is uniform doping, the net doping level is much greater than the intrinsic level and there is complete dopant ionization ($N_A^- \approx N_A$ and $N_D^+ \approx N_D$).[1] For n-channel this leads to

$$p_o = N_A \tag{A.9}$$

$$n_o = \frac{n_i^2 e^{-qV_{SB}/kT}}{p_o} \tag{A.10}$$

For p-channel the corresponding equations are

$$n_o = N_D \tag{A.11}$$

$$p_o = \frac{n_i^2 e^{-qV_{SB}/kT}}{n_o} \tag{A.12}$$

A.4 Surface Potential vs. Gate Voltage

The surface potential, ψ_s, varies depending on the gate voltage (V_g) applied to the device where

$$\psi_s = \frac{E_{iB} - E_{iS}}{q} \tag{A.13}$$

The bulk potential is defined as

$$\psi_F = \frac{E_{iB} - E_F}{q} \tag{A.14}$$

ψ_s is not however a direct function of the applied voltage, so some approximations must be used.

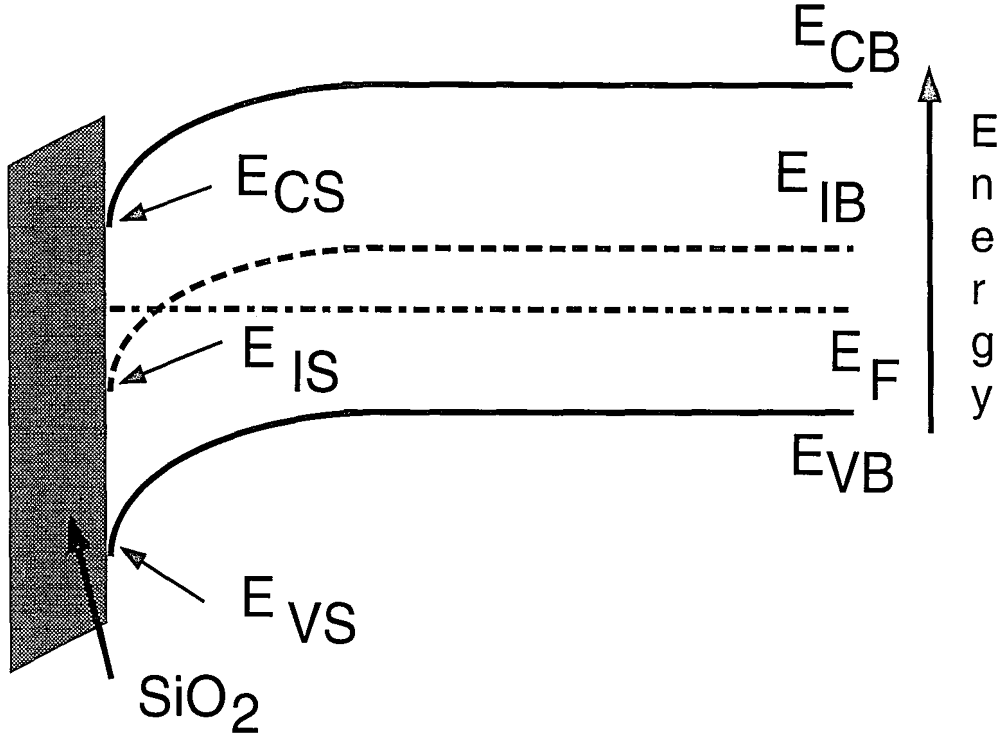

Figure A.3: Energy Bands of a n-channel semiconductor

Mode Name	Surface Potential	Gate Voltage
Accumulation	$-E_g/2q + \psi_F < \psi_s < 0$	$V_G < V_{FB}$
Flatband	$\psi_s = 0$	$V_G = V_{FB}$
Depletion	$0 < \psi_s < \psi_F$	$V_{FB} < V_G < V_{Tweak}$
Weak Inversion (Subthreshold)	$\psi_F < \psi_s < 2\psi_F$	$V_{Tweak} < V_G < V_T$
Strong Inversion	$2\psi_F < \psi_s < E_g/2q + \psi_F$	$V_G > V_T$

Table A.1: Regions of operations of a n-channel semiconductor

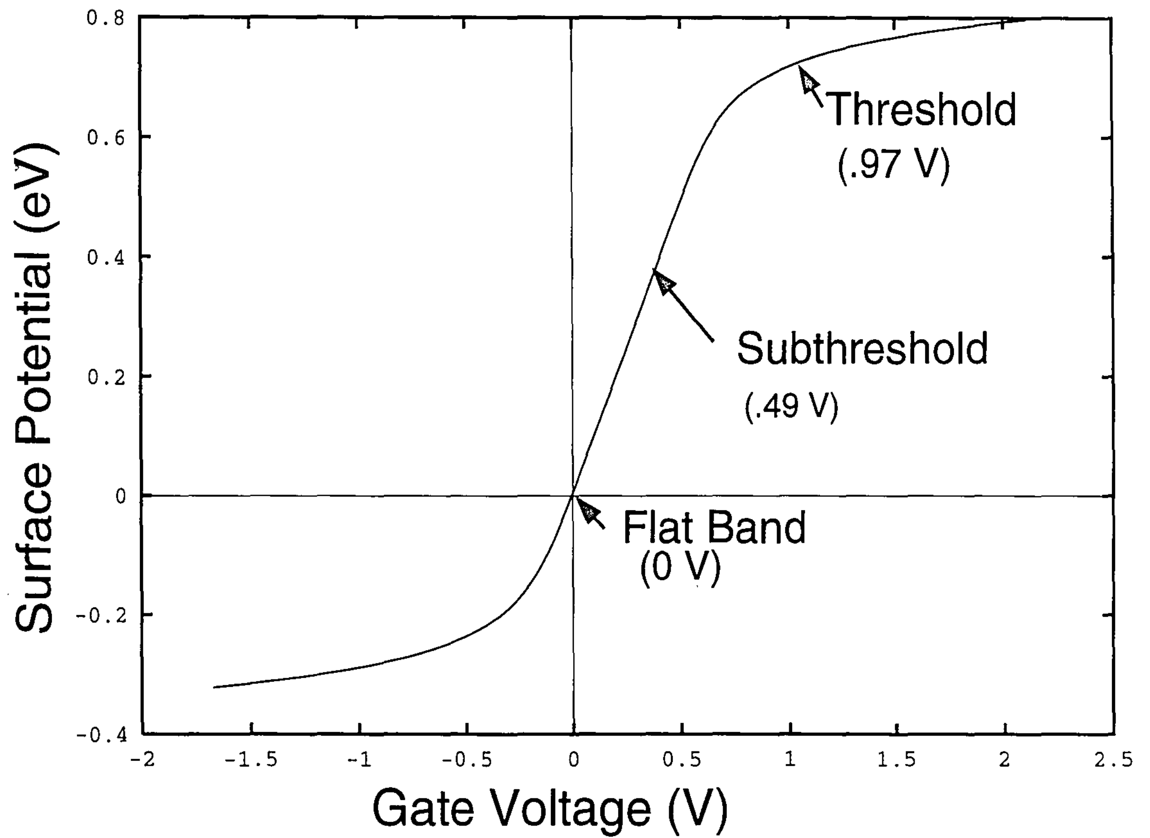

Figure A.4: Surface potential as a function of gate voltage at 300 K ($V_{SB} = 0$)

The gate charge conservation equation is[21]

$$V_g(t) = V_{FB} + \psi_s(t) - \frac{Q_s(\psi_s)}{C_{ox}} - \frac{Q_{it(\psi_t)}}{C_{ox}} \tag{A.15}$$

We assume that the interface charge ($Q_{it}(\psi_t)$) can be ignored, since,

$$\frac{Q_s(\psi_s)}{C_{ox}} \gg \frac{Q_{it}}{C_{ox}} \tag{A.16}$$

The oxide capacitor, C_{ox} is found from x_o, the oxide thickness by

$$C_{ox} = \frac{\epsilon_o k_o}{x_o} \tag{A.17}$$

The thermal voltage V_t is given as

$$V_t = \frac{kT}{q} \tag{A.18}$$

The semiconductor charge, Q_s, is given by

$$Q_s(\psi_s) = -\sqrt{2}\frac{kT}{q} f(\psi_s) K_s \epsilon_o \frac{\psi_s}{\left|\frac{\psi_s}{V_t} L_D\right|} \tag{A.19}$$

where

$$f(u_s) = \sqrt{e^{-u_s} + u_s - 1 + e^{-(2u_f + V_{SB})}(e^{u_s} - u_s e^{V_{SB}} - 1)} \tag{A.20}$$

The source to bulk bias is V_{SB}. and, assuming n-channel,

$$L_D = \sqrt{\frac{k_s \epsilon_o kT}{q^2 N_A}} \tag{A.21}$$

$$u_s = \frac{q\psi_s}{kT} \tag{A.22}$$

$$u_f = \frac{E_{iB} - E_f}{q} = \frac{kT}{q} \ln(\frac{N_A}{n_i}) \tag{A.23}$$

The total interface charge C_{it} is approximated by assuming it is constant, independent of ψ_t, for the purpose of determining ψ_s vs. V_g. It is given by

$$C_{it} = qD_{it} \tag{A.24}$$

[1]Incomplete Ionization or "freezeout" occurs mainly at low temperatures and high doping densities as the Fermi level comes close to the donor or acceptor level.[33, 34]

where D_{it} is the number of interface states per eV and cm^2. and ψ_s varies between ψ_{smax} and ψ_{smin} (to avoid degeneracy), where

$$\psi_{smax} = \frac{E_g}{2} + \psi_F \tag{A.25}$$

$$\psi_{smin} = -\frac{E_g}{2} + \psi_F \tag{A.26}$$

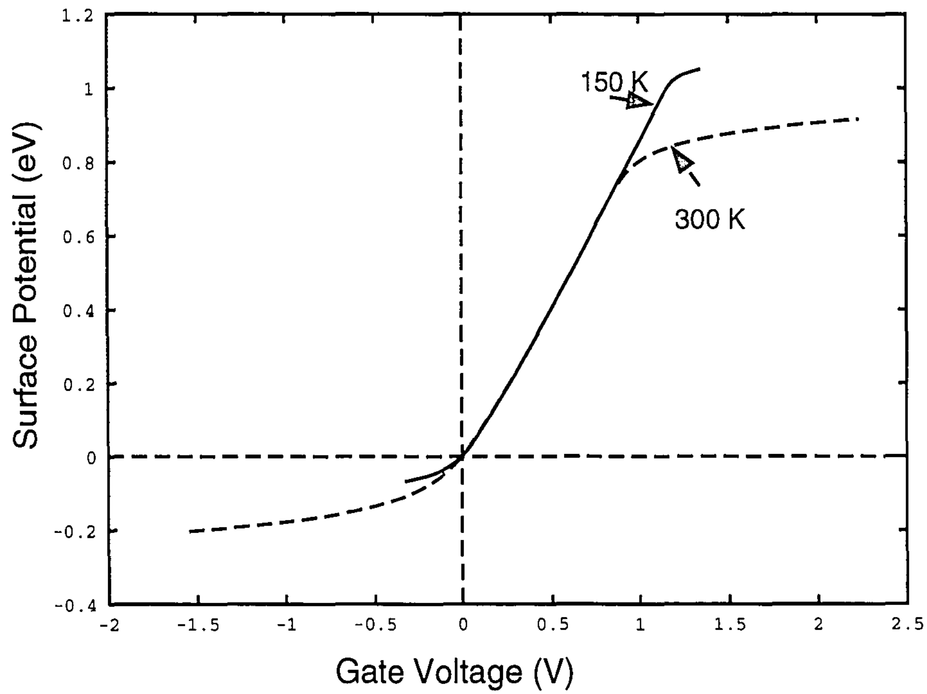

Figure A.5: Surface potential as a function of gate voltage at different temperatures

Appendix B

Fabrication Sequence

The MOS devices used in this study were fabricated by Dr. R. Siergiej following an abbreviated NMOS fabrication sequence[35, 36]. These devices were designed to study radiation effects.

B.1 The NMOS Processing Sequence

Positive fixed oxide charge induced by radiation tends to invert lightly doped p-substrates. Therefore, heavily doped p-substrate material (0.1-0.2 Ω-cm) was used. This process sequence is summarized below.

1. Starting material: p-$< 100 >$ 0.1-0.2 Ω-cm
   - Number device wafers
   - Number control wafers
2. Field Oxide, Active Device Regions: t_{ox}=5kÅ
   - RCA clean
   - High temperature oxidation. 5kÅ oxide: 1100°C, 50min

- Phtolithography: p$^+$ mask
- Buffered HF etch: 5kÅ oxide
- Strip photoresist: PRS-2000

3. Gate Electrode: ONO prepared in Triple Wall Oxide (TWO) system[37]

- RCA clean
- Flourinate: (optional) 1% HF, 5min
- High temperature TWO oxidation: POA in Argon ambient, 900°C, 15min
- LPCVD Nitride: 735°C, 250mTorr, 20sccm SiH_2Cl_2, 100sccm NH_3
- High temperature reoxidation of Nitride: 1000°C, steam, 50min
- LPCVD Polysilicon: 5kÅ, 625°C, 30min, 800mTorr, SiH_4 20% and N_2 80% mix, 180sccm
- Photolithography: polysilicon mask
- Plasma Etch: 5kÅ polysilicon; 250 Watts, 265mTorr, 100sccm SF_6
- Etch: Oxide, Buffered HF; Nitride, Hot phosphoric acid
- Strip photoresist: PRS-2000

4. n^+ Diffusion

- RCA clean
- High temperature diffusion: $POCl_3$, 900°C, 20min
- Diffusion drive-in: Nitrogen anneal; 900°C, 30min
- Strip P_2O_5 glass and pad oxide: Buffered HF etch

5. Contact Windows

- RCA clean
- High temperature wet oxidation: 1kÅ, 900°C, 18min

- Photolithography: Contact window mask
- Etch oxide: Buffered HF etch
- Strip photoresist: PRS-2000

6. Metallization

- Etch oxide: 1% HF solution
- Metallization: 7kÅ Aluminum, sputtered
- Photolithography: Metallization mask
- Etch: 7kÅ Aluminum, PAN etch, 45°C, 2min
- Strip photoresist: PRS-2000

7. Backside Metallization

- Spin photoresist on the front side
- Plasma etch: Backside, 300 Watts, 300mTorr, 100sccm SF_6
- Etch oxide: Buffered HF etch solution (backside)
- Metallization: 7kÅ Aluminum, evaporated
- Strip photoresist: PRS-2000

8. Post Metal Anneal

- Organic clean: 10min Acetone, 10min Methanol
- Nitrogen/Hydrogen Anneal: 350°C, 30min

Appendix C

Experimental Setup

C.1 Introduction

The experiments carried out in this lab are controlled by an HP9000 computer. The control program, FIDDLER, was written by Dr. Richard Booth and modified by many other students. This program allows data to be stored, manipulated and graphed on a printer or plotter.

C.2 Charge Pumping

The HP8115A pulse generator applies the pulse to the gate of the device under test. The source and drain are tied together and this is the current that is measured. The measured current is the electron current, while the current through the substrate is the hole current. As explained in the rest of the report the two currents differ only by sign.

A Keithley 616 Electrometer measures the current. The output is converted to digital and stored in the HP computer. Since the current is small care must be taken to remove any sources of noise and too keep the wires as short as possible. To further improve the measurements the surface of the devices is kept dry by nitrogen.

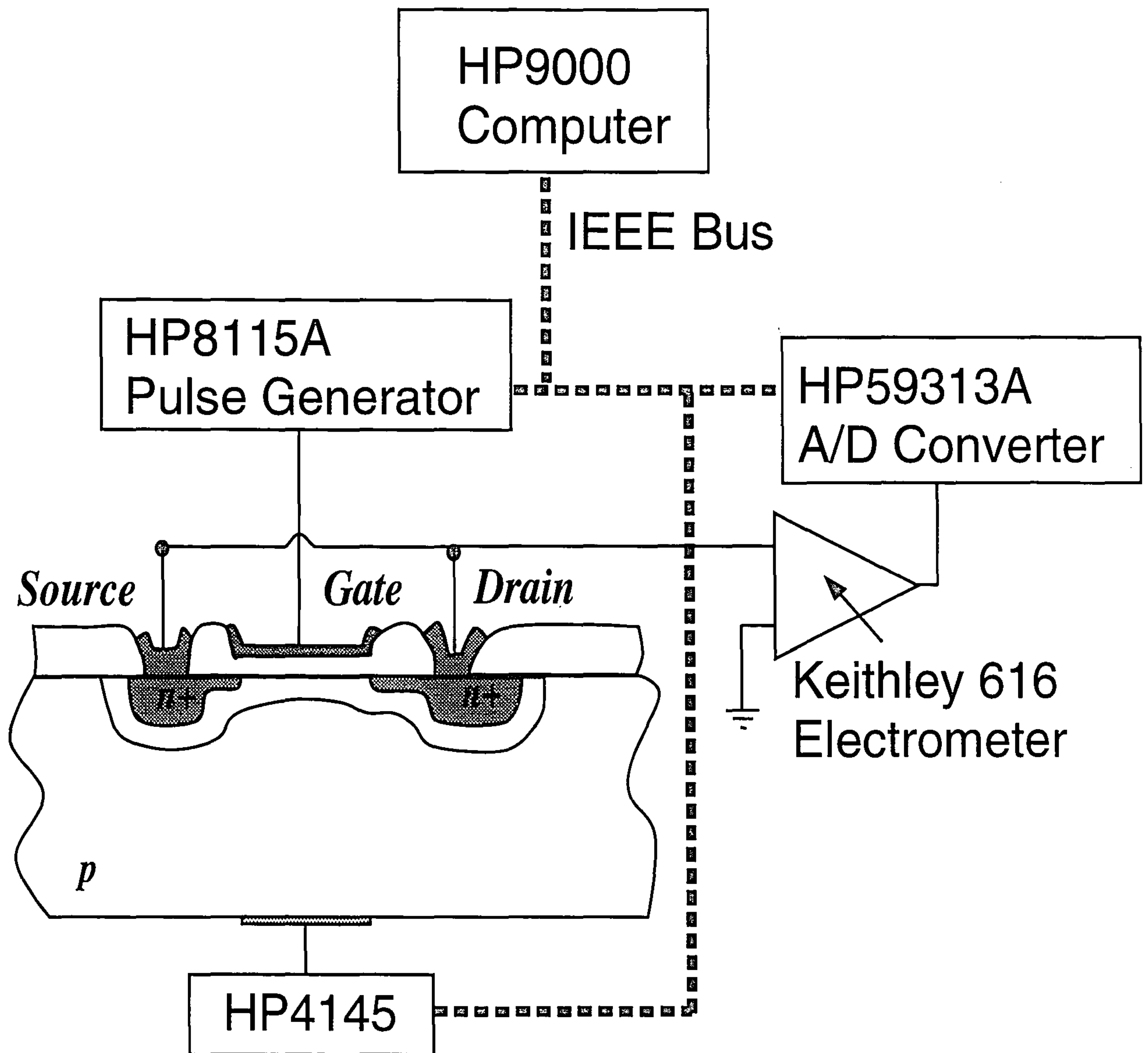

Figure C.1: Experimental setup

The Bulk bias is supplied by the HP4145.

C.3 Determination of Flatband Voltage

The program FLUTE[38, 39] extracts the threshold voltage and the bulk doping density. It also determines the the flatband voltage which is what we are interested in. The user supplies the width, length, t_{ox}, ξ (this is normally assumed equal to 1) and a guess for N_B. The device is measured using the HP-4145 and the HP computers. It uses a linear region parameter extraction method to compute the parameters of the device.

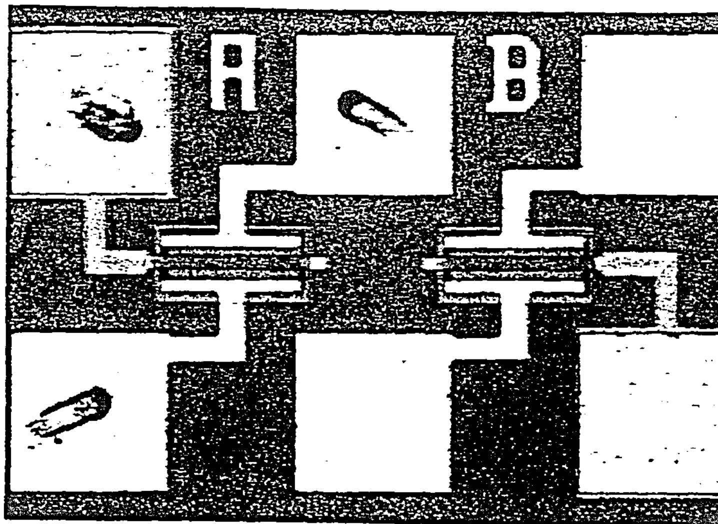

Figure C.2: The MOS transistor from the TP-300 mask set used in the experiments

Appendix D

Derivation of Equations

D.1 Capture and Emission Rates

The rate of capture for electrons by interface traps is the product of the capture coefficient ($\sigma_n v_{th}$), the number of free electrons at the surface (n_s), and the fraction of empty traps ($f_p(E)$). Where,

$$f_p(E) = 1 - f(E) \tag{D.1}$$

and $f(E)$ is the fraction of filled traps. This results in (for a single trap)

$$c_n = c_n^* f_p(E) n_s \tag{D.2}$$

where

$$c_n^* = \sigma_n v_{th} \tag{D.3}$$

The emission rate is given by, the emission coefficient (e_n^*) times the number of filled traps.

$$e_n = e_n^* f(E) \tag{D.4}$$

The emission rate can be found by considering the case of equilibrium. Fermi-Dirac statistics describe the the occupation probability, f, of occupancy in a trap at energy level E under equilibrium, with E_F the Fermi level as

$$f(E) = \frac{1}{1 + e^{(E-E_F)/kT}} \tag{D.5}$$

At equilibrium, the capture rate will equal the emission rate ($c_{no} = e_{no}$). The emission rate can be derived as follows:

$$c_{no} = e_{no} \tag{D.6}$$

$$\sigma_n v_{th} f_p(E) n_s = e_n^* f(E) \tag{D.7}$$

$$e_n^* = \sigma_n v_{th} n_s \frac{f_p(E)}{f(E)} \tag{D.8}$$

$$e_n^* = \sigma_n v_{th} n_s e^{(E-E_F)/kT} \tag{D.9}$$

since,

$$n_s = n_o e^{(E_{iB}-E_{iS})/kT} \tag{D.10}$$

we have,

$$e_n^* = \sigma_n v_{th} n_o e^{(E-E_F+E_{iB}-E_{iS}/kT} \tag{D.11}$$

By substituting equation D.11 into equation D.4, e_n can be written as:

$$e_n = \sigma_n v_{th} n_o e^{q\psi_t/kT} f(E) \tag{D.12}$$

As long as the device is close to equilibrium, the equilibrium rates can be used ($c_n \approx c_{no}$ and $e_n \approx e_{no}$). The equations for the hole emission and capture can be found in a similar manner.

$$c_p = \sigma_p v_{th} p_s f(E) \tag{D.13}$$

$$e_p = \sigma_p v_{th} p_o e^{-q\psi_t/kT} \tag{D.14}$$

D.2 Electron and Hole Currents

The electron and holes flowing into and out of the traps lead to a current flow. The electrons lead to the electron current (j_n) and the holes cause the hole current

(j_p). To find the equations for these currents, we first find the generation rate (G) for steady state. In general

$$\frac{df}{dt} = (c_n - e_n) - (c_p - e_p) \tag{D.15}$$

and

$$G = \frac{df}{dt} \tag{D.16}$$

If we look at steady state,

$$\frac{df}{dt} = 0 \tag{D.17}$$

which leads to

$$c_n - e_n = c_p - e_p \tag{D.18}$$

By substituting equations D.2, D.13, D.12 and D.14 into the above, one has

$$c_n^* n_s(1 - f_{ss}) - e_n^* p_s f_{ss} = c_p^* f - e_p^*(1 - f_{ss}) \tag{D.19}$$

Solving for f_{ss},

$$f_{ss} = \frac{c_n^* n_s + e_p^*}{e_n^* n_s + c_p^* + e_n^* p_n + e_p^*} \tag{D.20}$$

By placing the results of equation D.20 into equation D.16, the expression for G becomes,

$$G = \frac{n_i^2 - np}{\frac{n + n_1}{\sigma_p v_{th}} + \frac{p + p_1}{\sigma_n v_{th}}} \tag{D.21}$$

The region of interest is the depletion mode, since we are interested in the times when the gate voltage is above the flatband voltage, but below the threshold voltage. In this region there are few free carriers, so $n \approx p \approx 0$. This allows G to be simplified to

$$G = \frac{\sigma_n \sigma_p v_{th} n_i}{\sigma_n e^{(E_t - E_{iS})/kT} + \sigma_p e^{(E_{iS} - E_t)/kT}} \tag{D.22}$$

Recalling that the pinning level E_{TP} can be expressed as

$$E_{TP} = E_{iS} - \frac{1}{2} kT \ln(\frac{\sigma_n}{\sigma_p}) \tag{D.23}$$

G can be expressed as

$$G = \frac{kT\sqrt{\sigma_n\sigma_p}v_{th}n_i}{e^{(E_T-E_{TP})/kT} + e^{-(E_T-E_{TP})/kT}} \tag{D.24}$$

$$G = \frac{kT\sqrt{\sigma_n\sigma_p}v_{th}n_i}{2cosh(E_T - E_{TP})} \tag{D.25}$$

Equation D.25 applies to a single trap at energy level E_T, since there are interface traps at all the energy levels between E_V and E_C, (D.25) must be integrated over the entire energy gap to find the current density. If we assume the capture cross sections are constant over the energy gap, we have

$$J = q\int_{E_V}^{E_C} G(E_T)\,dE_T \tag{D.26}$$

$$J = \frac{kT}{2}q\sqrt{\sigma_n\sigma_p}v_{th}n_i\int_{E_V}^{E_C}\frac{dE_T}{cosh(E_T - E_{TP})} \tag{D.27}$$

Since $\frac{1}{cosh(E_V-E_{TP})} \ll 1$ and $\frac{1}{cosh(E_C-E_{TP})} \ll 1$, we can let $E_V \to -\infty$ and $E_C \to \infty$ in equation D.27.

$$J = \frac{kT}{2}q\sqrt{\sigma_n\sigma_p}v_{th}n_i\int_{-\infty}^{\infty}\frac{dE_T}{cosh(E_T - E_{TP})} \tag{D.28}$$

This equation can be evaluated analytically to give,

$$J = \frac{KT}{2}q\sqrt{\sigma_n\sigma_p}v_{th}n_i\pi \tag{D.29}$$

So, the effective current of all the interface traps is $\frac{\pi}{2}$ times the amount due to the trap at the pinning level. We assume that this approximation holds for the non-steady state conditions encountered during the simulations.

Appendix E

Time of Simulations

The simulations were carried out on various workstations and the results were compared. The Unix *time* command was used to record the results. The times listed below are the user times. The user times are the time the machine spent executing that particular program. Since more than one program can be running at a time, the time a user would have to wait is often much longer. In theory the user time should be independent of the number of other users; however, this is not the case since programs may need to be swapped into and out of memory and the hard disk if the load is too high. This explains why *cs1.cc* was slower than *cs2.cc* even though *cs1.cc* is the faster machine. The IBM machines run under the AIX operating system. The Sun machines use SunOs. Both are versions of the Unix operating system.

Machine Name	Model	Time (seconds)
Calvin.sfc	Sun Sparc 1	10.2
Hobbes.sfc	Sun Sparc SLC	10.5
Spiff.sfc	Sun Sparc IPC	8.9
Cs1.cc	IBM RS 6000 950	1.52
Cs2.cc	IBM RS 6000 580	.86

Table E.1: Comparison of User times for simple two-level simulation on various machines

The time required for the different simulation experiments was also calculated. The time required for the full tri-level simulations were several days on the Sun Workstations. For this reason, it is suggested that the programs be run using the

Unix *nice* command which allows a user to lower the priority of their process so other users will not be slowed down as much. Even running with a reduced priority other users will notice the slow down of the machine so the longer simulations should be run at night or on weekends.

Simulation	Waveforms saved?	Time (minutes)
Bi-level	yes	1:01
Tri-level	yes	5:17
Tri-level	yes	25:51

Table E.2: Comparison of User times for different simulations on *ratool.*

Appendix F

Source Code

The C source code for the program used in the simulations is shown below. The C language is case sensitive, and it does not allow Greek symbols. Traditionally, constants are specified as all caps and variables and functions are in all lower case. This practice was followed in this program. The *pump.h* file is the header file. It contains the constants used in the simulation. The user can edit this file to change the characteristics of the device in the simulations. If the header file or the program is changed, the program must be recompiled. To compile the program, the user types `cc -o pump.out -O pump.c` at the unix prompt. The program is then run by typing `pump.out`.

F.1 pump.h

```
/* pump.h for use with pump.c*/
/*Define the constants used in the program*/
#define NA 5e16
#define DIT 1e10
/*3D Capture Cross Sections*/
#define SP3D 1e-17
#define SN3D 1e-17
/*Flatband voltage*/
#define VFB 0
#define XO 1.95e-6
/*1e-6*/
/*Temperature*/
#define T 300.0
/*Number of times to run through waveform*/
#define COUNT 1
/*Number of points in PSIs vs. Vg curve*/
#define POINTS 1000
#define VSB 0.0
#define ALPHA .5
```

F.1. PUMP.H

```
/* Uncomment the following line to have the program print out the
waveforms of the currents, potentials and voltages.*/
/**#define WAVEFORM*/

/*Uncomment out the following line to include quantization effects*/
#define QUANTUM

/*Uncomment the following line to include debugging information*/
#define DEBUG
```

F.2 pump.c

```
/* This program simulates Tri-level charge pumping
Written by Bill Wagner*/
#include <stdio.h>
#include <stdlib.h>
#include <math.h>

#include "pump.h"

/*Thermal velocity*/
#define K 1.38e-23
#define Q 1.6e-19
#define CIT Q*DIT
#define VT (K*T/Q)
#define KS 11.7
#define KO 3.9
#define EO 8.854e-14
#define LD sqrt((VT*KS*EO)/(Q*NA))
#define COX (EO*KO/XO)
#define TSTART 1e-9
#define ERROR 1e-8
#define MO 9.11e-31
#define MN (1.08*MO)
#define MP (.81*MO)
#define ML (.98*MO)
#define PI 3.14159
#define H 6.625e-34

/*T1, T2 and T3 are the length of the step*/
#define T1 1.1e-5
#define T2 .5e-6

/*The following are the transition times for the various steps*/
#define TR1 10e-9
#define TR2 10e-9
#define TR3 10e-9
/*These are the voltages of the various steps*/
#define V1 1.5
#define V2 -.5
#define VL -0.5
#define VH .5
#define DV 2.0
#define VS .1
#define HBAR ((H)/(2.0*PI))

double VTH,NI,EG,UF,PSISMIN,PSISMAX,NO,SP,SN;

/*Calculate Constants*/
void calc_constants ()
{
  double deg,nc,nv,sigma,alpha,eo;

  VTH=sqrt(8*K*T/(PI*MN))*100.0;
  EG=1.170-(4.73e-4 * T*T)/(T+636);
  deg=(3*Q*Q/(16.0*PI*KS*EO))*sqrt((Q*NA)/(KS*EO*K*T));
  EG-=deg;
  nc=2.0*pow((2.0*PI*MN*K*T/(H*H)),1.5)/1e6;
  nv=2.0*pow((2.0*PI*MP*K*T/(H*H)),1.5)/1e6;
  NI=sqrt(nc*nv)*exp(-EG*Q/(2*K*T));
  UF=log(NA/NI);
  PSISMIN=-EG/2.0+UF*VT;
  PSISMAX=EG/2.0+UF*VT;
  PO=NA;
  NO=(NI*NI*exp(-1.0*VSB)*exp(-1.0*VSB))/PO;
  SP=SP3D;
  SN=SN3D;
```

```
/* Use Quantun effects only if quantum defined */
  alpha=pow(HBAR*HBAR*Q*NA/(ML*KS*E0),(1.0/3.0))*pow(9.0*PI*Q/8.0,2.0/3.0);
  eo=alpha*pow(2*K*T*UF/Q+VSB,(1.0/3.0))/(K*T);
  sigma=3.55*exp(Q*eo/(K*T))/sqrt(Q*eo/(K*T));
#ifdef QUANTUM
  SN *=sigma;
#endif
#ifdef DEBUG
  printf ("NI=%g EG=%g VTH=%g UF=%g\n",NI,EG,VTH,UF);
  printf ("sigma ratio=%g alpha=%g eo=%g\n",sigma,alpha,eo);
  if (SN!=SN3D) printf ("Quantum effects included\n");
#endif
}

/*Calculate the hole current given PSIt and PSIs*/
double calc_jp (psit,psis)
double psit,psis;
{
  double cp,ep;

  cp=SP*VTH*P0*exp(-Q*psis/(K*T));
  ep=SP*VTH*P0*exp(-Q*psit/(K*T));
  return (VT*CIT*(cp-ep));
}

/*Calculate the electron current given PSIt and PSIs*/
double calc_jn (psit,psis)
double psit,psis;
{
  double cn,en;

  cn=SN*VTH*N0*exp(Q*psis/(K*T));
  en=SN*VTH*N0*exp(Q*psit/(K*T));
  return (VT*CIT*(en-cn));
}

/*Calculate the change in PSIt from the previous point*/
double calc_dpsit (psit,psis)
double psit,psis;
{
  double cp,cn,ep,en;

  cp=SP*VTH*P0*exp(-Q*psis/(K*T));
  cn=SN*VTH*N0*exp(Q*psis/(K*T));
  ep=SP*VTH*P0*exp(-Q*psit/(K*T));
  en=SN*VTH*N0*exp(Q*psit/(K*T));
  return (VT*(cn-en+ep-cp));
}

/* The following 4 subroutines are used to generate the psis-vg table*/
double f(us)
double us;
{
  double t1,t2;

  t1=exp(-us)+us-1.0;
  t2=exp(-2.0*UF-VSB)*(exp(us)-us*exp(VSB)-1.0);
  return(sqrt(t1+t2));
}

double qs(psist)
double psist;
{
  return (-sqrt(2.)*VT*f(psist/VT)*KS*E0*(psist/VT)/(fabs(psist/VT)*LD));
}

double calc_vg(psist)
double psist;
{
  return (VFB+psist-qs(psist)/COX-CIT/COX);
```

```
}

void calc_vgtpsis (vgtest,psist)
double vgtest[],psist[];
{
  int i;

  for (i=0;i<POINTS;i++) {
    psist[i]=PSISMIN+(PSISMAX-PSISMIN)*(1.0*i/POINTS);
    vgtest[i]=calc_vg(psist[i]);
  }
}

/* The following subroutine returns psis for the given gate voltage*/
double calc_psis (vg,vgtest,psist)
double vg,vgtest[],psist[];
{
  int i;
  double t;

  if (vg<vgtest[0]) return (psist[0]);
  for (i=1;i<POINTS;i++) {
    if (vg<vgtest[i]) {
      t=vgtest[i]-vgtest[i-1];
      return (psist[i-1]+(psist[i]-psist[i-1])*(vg-vgtest[i-1])/t);
    }
  }
  return (psist[POINTS-1]);
}

/* Return the gate voltage for a given time t. */
double return_vg (t,t1,t2,t3,tr1,tr2,tr3,v1,v2,v3)
double t,t1,t2,t3,tr1,tr2,tr3,v1,v2,v3;
{
  double vg;

/* The gate voltage is at V2 at time 0
   It changes to V1 over tr1
   It stays at V1 for t1
   It changes to V3 over tr2
   it stays at V3 for t3
   It changes to v2 over tr3
   It stays at v2 for the rest of the cycle */

/* First make sure time is reflected back into the first time period
   since vg(t+period)=vg(t) */
  while (t>=t1+t2+t3+tr1+tr2+tr3) t-=(t1+t2+t3+tr1+tr2+tr3);
  vg=v2;
  if (t<=tr1+t1) vg=v1;
  if ((t>=tr1+t1+tr2) && (t<=tr1+t1+tr2+t3)) vg=v3;
  if (t<tr1) vg=t/tr1*(v1-v2)+v2;
  if ((t>tr1+t1) && (t<tr1+t1+tr2)) vg=(t-tr1-t1)/tr2*(v3-v1)+v1;
  if ((t>tr1+t1+tr2+t3) && (t<tr1+t1+tr2+t3+tr3))
    vg=(t-tr1-t1-tr2-t3)/tr3*(v2-v3)+v3;
  return (vg);
}

/* The following subroutine opens up an output file, checks that the file
is opened properly and writes the user supplied constants to the file*/
FILE *fwopen (s)
char *s;
{
  FILE *out;

  out=fopen (s,"w");
  if (out==NULL) {
    printf ("Can't open file %s\n",s);
    exit (-1);
  }
#ifdef DEBUG
```

```
  printf ("Opened file %s\n",s);
#endif

  fprintf (out,"# %s\n",s);
  fprintf (out,"#NA=%g COUNT=%d temp=%g points=%d\n",NA,COUNT,T,POINTS);
  fprintf (out,"#VSB=%g DIT=%g XO=%g\n",VSB,DIT,XO);
  fprintf (out,"#SP3D=%g SN3D=%g\n",SP3D,SN3D);
#ifdef QUANTUM
  fprintf (out,"#QUANTUM EFFECTS INCLUDED\n");
#endif
  return(out);
}

/* The following subroutine calculates the total charge for a complete
waveform */
double calc_i (t1,t2,t3,tr1,tr2,tr3,v1,v2,v3,vgtest,psist,error)
double t1,t2,t3,tr1,tr2,tr3,v1,v2,v3,vgtest[],psist[],*error;
{
  double t,tstep,tstepmax,icp1,icp2,jp1,jp2,jp3,jn1,jn2,jn3,jp,jn;
  double ovg,opsis,opsit,vg,psis,psit,vga,psisa,psita,dpsit,check,e;
  int i,test;
  FILE *out1,*out2,*out3,*out4,*out5;

#ifdef WAVEFORM
  out1=fwopen ("vg.dat");
  out2=fwopen ("psis.dat");
  out3=fwopen ("psit.dat");
  out4=fwopen ("jn.dat");
  out5=fwopen ("jp.dat");
#endif

  tstep=tr1/25.0;
#ifdef WAVEFORM
  tstep=tr1/250.0;
#endif
  if (t1==0) tstep/=2000.0;
/*Set max. step size*/
  tstepmax=4.0*tstep;
  t=tstep;
  ovg=return_vg (0.0,t1,t2,t3,tr1,tr2,tr3,v1,v2,v3);
  opsis=calc_psis (ovg,vgtest,psist);
  opsit=opsis;

#ifdef WAVEFORM
  fprintf (out1,"%g %g\n",0.0,ovg);
  fprintf (out2,"%g %g\n",0.0,opsis);
  fprintf (out3,"%g %g\n",0.0,opsit);
#endif

/*Start calculations*/
  icp1=icp2=0.0;
  for (i=1;(t<COUNT*(tr1+t1+tr2+t3+tr3+t2))&&(i>0);i++) {
    test=2;
    do {
      vg=return_vg (t,t1,t2,t3,tr1,tr2,tr3,v1,v2,v3);
      psis=calc_psis (vg,vgtest,psist);

      vga=return_vg (t-tstep/2.,t1,t2,t3,tr1,tr2,tr3,v1,v2,v3);
      psisa=calc_psis (vga,vgtest,psist);
      psita=opsit+calc_dpsit (opsit,opsis)*tstep/2.0;
      check=psita+calc_dpsit (psita,psisa)*tstep/2.0;
      psit=opsit+calc_dpsit(opsit,opsis)*tstep;
      if (test==0) test=1;
      if (fabs(psit-check)>((PSISMAX-PSISMIN)/1000.0)) {
          test=0;
  tstep/=10.;
  t-=9.*tstep;
      }
    } while (test==0);
    ovg=vg;
```

```
    jp1=calc_jp(opsit,opsis);
    jn1=calc_jn(opsit,opsis);
    jp2=calc_jp(psita,psisa);
    jn2=calc_jn(psita,psisa);
    jp3=calc_jp(psit,psis);
    jn3=calc_jn(psit,psis);
    jp=(jp1+4.0*jp2+jp3)/6.0;
    jn=(jn1+4.0*jn2+jn3)/6.0;
    icp1+=jp*tstep;
    icp2+=jn*tstep;
    opsis=psis;
    opsit=psit;
    if (test==2) tstep*=5.0;
    if (tstep>tstepmax) tstep=tstepmax;

#ifdef WAVEFORM
    fprintf (out1,"%g %g\n",t,vg);
    fprintf (out2,"%g %g\n",t,psis);
    fprintf (out3,"%g %g\n",t,psit);
    fprintf (out4,"%g %g\n",t,jn3);
    fprintf (out5,"%g %g\n",t,jp3);
#endif

    t+=tstep;
  }
#ifdef WAVEFORM
  fclose (out1);
  fclose (out2);
  fclose (out3);
  fclose (out4);
  fclose (out5);
#endif

  e=fabs(icp1+icp2)/2.0;
  *error=e*1e9/COUNT;
/*  if (20*e>fabs(icp1)||20*e>fabs(icp2)) {
    return (-1.0);
  }
  else */return ((icp1-icp2)*.5e9/COUNT);
}

void varyfreq (vgtest, psist)
double vgtest[], psist[];
{
  FILE *out1;
  double freq,t1,t2,e1,tcur1;

  out1=fwopen("currf.dat");
  fprintf (out1,"#v1=%g v2=%g\n",V1,V2);
  fprintf (out1,"#ALPHA=%g TR1=%g TR2=%g\n",ALPHA,TR1,TR2);
  for (freq=1.0e6;freq<2.0e6;freq*=100.0) {
    t1=ALPHA/freq;
    t2=(1.0-ALPHA)/freq;
/* Use the following line for sawtooth waves*/
/*    tcur1=calc_i (0.0,0.0,0.0,t1,t2,0.0,V1,V2,V2,vgtest,psist,&e1);*/
    t1=.5/freq-(TR1+TR1)/2.0;
/* Use the following line for square waves*/
    tcur1=calc_i (t1,t1,0.0,TR1,TR2,0.0,V1,V2,V2,vgtest,psist,&e1);
    if (tcur1==-1.0) {
      fprintf (out1,"#%g problem\n",freq);
      fflush (out1);
    }
    else {
      fprintf (out1,"%g %g %g\n",freq,tcur1,e1);
      fflush (out1);
    }
  }
  fclose (out1);
}
```

```
void varyBase (vgtest,psist)
double vgtest[], psist[];
{
  FILE *out1;
  double e1, tcur1, v3;

  out1=fwopen("currf.dat");
  fprintf (out1,"#delta v=%g\n",T,DV);
  fprintf (out1,"#T=%g TR1=%g TR2=%g\n",T,TR1,TR2);
  for (v3=VL;v3<=VH;v3+=.05) {
    tcur1=calc_i (T1,T1,0.0,TR1,TR2,0.0,v3+DV,v3,v3,vgtest,psist,&e1);
    if (tcur1==-1.0) {
      fprintf (out1,"#%g problem\n",v3);
      fflush (out1);
    }
    else {
      fprintf (out1,"%g %g %g\n",v3,tcur1,e1);
      fflush (out1);
    }
  }
  fclose (out1);
}

void tri (vgtest,psist)
double vgtest[], psist[];
{
  FILE *out1;
  double e1, e2, cur, t1,t2, ts, tcur1, tcur2, v3;

  out1=fwopen("testall.dat");
  fprintf (out1,"#TR1=%g TR2=%g TR3=%g\n",TR1,TR2,TR3);
  fprintf (out1,"#V1=%g V2=%g\n",V1,V2);


  for (v3=1.3;v3<=1.4;v3+=10.0) {
    fprintf (out1,"\n#v3=%g\n",v3);
    tcur1=calc_i (T1,T1-TSTART,TSTART,TR1,TR2,TR3,V1,V2,v3,vgtest,psist,&e1);
    if (tcur1==-1.0) {
      fprintf (out1,"#%g problem\n",TSTART);
      fflush (out1);
    }
    else {
      fprintf (out1,"%g %g %g\n",TSTART,tcur1,e1);
      fflush (out1);
      t1=TSTART;
      for (t2=TSTART*100.0;t2<T1;t2*=100.0) {
tcur2=calc_i (T1,T1-t2,t2,TR1,TR2,TR3,V1,V2,v3,vgtest,psist,&e2);
if (tcur2==-1.0) {
  fprintf (out1,"#%g problem\n",t2);
  fflush (out1);
}
else {
  if (fabs(tcur2-tcur1)<1e-6) {
    fprintf (out1,"%g %g %g\n",t2,tcur2,e2);
    fflush (out1);
    t1=t2;
  }
  else {
    for (ts=t1*1.77827941;ts<(t2*.90);ts*=1.77827941) {
      cur=calc_i (T1,T1-ts,ts,TR1,TR2,TR3,V1,V2,v3,vgtest,psist,&e1);
      if (cur==-1.0) {
fprintf (out1,"#%g problem\n",ts);
fflush (out1);
      }
      else {
fprintf (out1,"%g %g %g\n",ts,cur,e1);
fflush (out1);
      }
    }
    tcur1=tcur2;
```

```
    t1=t2;
    fprintf (out1,"%g %g %g\n",t2,tcur2,e2);
    fflush (out1);
  }
}
      }
      t1=t2;
      for (ts=t1*1.77827941;ts<T1;ts*=1.77827941) {
        cur=calc_i (T1,T1-ts,ts,TR1,TR2,TR3,V1,V2,v3,vgtest,psist,&e1);
if (cur==-1.0) {
  fprintf (out1,"*%g problem\n",ts);
  fflush (out1);
}
        else {
  fprintf (out1,"%g %g %g\n",ts,cur,e1);
  fflush (out1);
}
      }
    }
  }
}

/**** Main Program Starts Here*****/
main ()
{
  double vgtest[POINTS],psist[POINTS];
  double tcur,e;
  FILE *out1;
  int i;

  calc_constants ();
/*Calc the curve of VG vs. PSIt*/
  calc_vgtpsis(vgtest,psist);
/* Uncomment out the following lines to save PSIs vs Vg Data to output file*/
  out1=fwopen ("vgt.dat","w");
  for (i=0;i<POINTS;i++) {
    fprintf (out1,"%g %g\n",vgtest[i],psist[i]);
  }
  fclose (out1);

/*Uncomment out the line below corresponding to the waveform to use*/
/*   varyfreq (vgtest,psist);*/
/*  varybase (vgtest,psist);*/
/*  tri (vgtest,psist);*/
/*    tcur=calc_i (2e-7,2e-7,.5e-5,TR1,TR2,TR3,V1,V2,.8,vgtest,psist,&e);
  printf ("%g %g\n",tcur,e);*/
}
```

Vitae

William E. Wagner was born July 2, 1970 to Dr. and Mrs. William Wagner, Jr in Basking Ridge, NJ. He started Lehigh University in the fall of 1987 and graduated with honors with a B.S.E.E. degree in June 1991. He was adwarded a Sherman Fairchild Fellowship for the 1992-93 and 94-94 school years. He is currently working toward his PhD degree in Microelectronics. He lives in Bethlehem with his dog Lucky.

END

OF

TITLE